NATIONAL ADVISORY COMMITTEE FOR AERONAUTICS

TECHNICAL NOTE 3266

EXPERIMENTAL EVALUATION OF MOMENTUM TERMS IN TURBULENT PIPE FLOW

By Virgil A. Sandborn

Lewis Flight Propulsion Laboratory
Cleveland, Ohio

Washington
January 1955

Z

NATIONAL ADVISORY COMMITTEE FOR AERONAUTICS

TECHNICAL NOTE 3266

EXPERIMENTAL EVALUATION OF MOMENTUM TERMS IN TURBULENT PIPE FLOW

By Virgil A. Sandborn

SUMMARY

The mean and turbulent momentum terms in fully developed turbulent pipe flow were experimentally evaluated. The terms of the longitudinal-direction momentum equation, obtained from the Reynolds equations of turbulent fluid motion, were experimentally evaluated in a 4-inch-diameter pipe from total- and static-pressure data and hot-wire anemometer surveys. Measurement of the terms appearing in the radial-direction momentum equation indicates the existance of terms as large as or larger than the terms of the longitudinal-direction momentum equation.

Analysis of the turbulent stress tensor shows that the direction of principal stress was oriented nearly parallel to the wall in the region near the wall. Variation with Reynolds number of the longitudinal turbulent intensity at the center of the pipe indicates that the intensity at the center was of a universal nature.

A direct comparison was made with turbulence measurements obtained using the constant-current and constant-temperature systems of hot-wire anemometry. The two systems agree well within the experimental accuracy of the measurements. The constant-temperature measurements also agree with the measurements of turbulence presented by Laufer for the same Reynolds number.

INTRODUCTION

Although turbulence in aerodynamics is of greatest importance in connection with boundary layers, basic experimental or theoretical studies of the boundary layer entail many difficulties. It has proven more practical mathematically and experimentally to investigate the simpler forms of turbulent shear flow, such as fully developed pipe and channel flows. Detailed study of these simpler flows may lead to a better understanding of the behavior of turbulent boundary layers.

Results of measurements of turbulent flow in a pipe and a channel have recently been reported in references 1 and 2. Results of further measurements made in a fully developed pipe flow are presented herein. These measurements were made not only as an independent verification of the results of reference 1, but also as a comparison between two distinct systems of hot-wire anemometry.

Measurements were made in a 4-inch-diameter pipe, which was originally built to facilitate the development and calibration of hot-wire equipment at the NACA Lewis laboratory. The Reynolds number range (based on pipe radius) was from approximately 20,000 to 200,000. The measurements are similar to those reported in reference 1, but include only the mean and statistical quantities necessary to evaluate the terms in the Reynolds equations of motion.

The two types of hot-wire anemometry equipment were the constant-current (or constant-mean-resistance) system and the constant-temperature system. In the past, the constant-current system with compensating a-c amplifier has been used almost exclusively for the measurement of turbulence because a preliminary analysis (ref. 3) indicated that the noise level of the constant-temperature system would be prohibitively high. However, refinements in the system have reduced the noise level of the constant-temperature system to a point comparable with that of the constant-current system. The actual recording of turbulence data is, by comparison, much simpler with the constant-temperature system.

APPARATUS AND PROCEDURE

Test facility. - The test facility consisted of a 4-inch-inside-diameter seamless aluminum pipe 19.5 feet in length connected to an air supply through a settling chamber and a series of filters, screens, and a honeycomb arrangement, as shown in figure 1. Room air, filtered through Fiberglas air filters, was supplied by a constant-speed centrifugal blower and was metered by a 4-inch valve. As experimental work proceeded, it was necessary to add an increasing number of paper air filters in the system to prevent dirt particles from affecting the hot-wire measurements. The maximum Reynolds number was 200,000 when measurements were started, but as more filtering was added the maximum Reynolds number was reduced to about 150,000 in the region where fully turbulent flow was obtained. Data were taken at Reynolds numbers of 25,000, 50,000, 100,000, and 150,000.

Mean velocity instrumentation. - The mean velocity measurements were made with a total-pressure probe having a 0.040-inch outside diameter (with a wall thickness of approximately 0.003 in.) flattened to 0.010 inch at the tip so that surveys could be made to a point 0.005

inch from the pipe wall. The probe was accurately positioned at the wall by use of an electrical contact indicator; surveys were made at a position 14 inches from the pipe exit.

Total pressures were recorded continuously by differential pressure transducers, which were referenced to atmospheric pressure. The two transducers employed had full-scale pressure ranges of ±0.05 pound per square inch and ±0.15 pound per square inch, with their outputs being recorded on a 2-millivolt full-scale recording potentiometer. In the systems employed it was possible to detect pressure differences of the order of 0.004 pound per square foot and 0.01 pound per square foot, respectively, for the two instruments. A more elaborate description of the transducing systems is given in reference 4.

It has been found experimentally (ref. 5) that total-pressure-probe corrections are necessary at very low velocities. In the course of measurements in the pipe, it was possible to determine a correction for the total-pressure-probe error by comparing measurements of the velocities obtained from hot-wire and total-pressure probes at the center of the pipe for very low Reynolds numbers. The correction resulted in an increase in measured velocity of 15 percent at 10 feet per second. Therefore, the low velocities in the region near the pipe wall were corrected for the probe error. No corrections were made for probe displacement effects due to total-pressure gradients.

Static-pressure instrumentation. - The pipe was equipped with wall static taps along the top. The taps were equally spaced 2 inches apart in the region where surveys were taken and 4 inches apart upstream. The pressure distributions for Reynolds numbers of 25,000 and 50,000 are shown in figure 2. A slight blockage effect was observed when probes were mounted in the pipe, and corrections were made in evaluating the mean velocity and the wall shearing stress as the probe position was varied. These corrections were the result of a maximum increase in static pressure of 8 to 10 percent as the probe was moved from the wall to the center of the pipe.

Hot-wire turbulence-measuring equipment. - Turbulent fluctuation measurements have been made with two independent systems of hot-wire anemometry. Both the constant-mean-current and constant-instantaneous-temperature systems were employed in the measurement of the turbulent velocity fluctuations, mainly in an attempt to determine the validity of employing the constant-temperature system for boundary layer research.

The constant-current system (fig. 3) was basically that employed by the National Bureau of Standards (ref. 6). The circuit consists of a noninductive-type Wheatstone bridge and an a-c amplifier equipped with a variable resistance-capacitance network to compensate for thermal lag of a hot wire. The thermocouple RF meter circuit used to obtain a measure

of the mean square of the fluctuating voltage is also included in figure 3. Figure 4 shows the gain with frequency of the complete anemometer system with a wire installed in the bridge, both with amplifier compensation and without compensation.

The constant-temperature system is that described in reference 7 with minor changes made to reduce the over-all noise level of the system. The output of the constant-temperature anemometer was read on the average-square computers described and evaluated in reference 7. An outline of the connections used to obtain the data necessary to evaluate the statistical averages of the turbulent quantities is included in reference 4.

A wiring diagram of the sum and difference circuit employed in the measurements of $\sqrt{\overline{v^2}}$ and $\sqrt{\overline{w^2}}$ is shown in figure 5. This sum and difference circuit has proven superior to the circuit reported in reference 7, for the noise level and thus the difference minimum has been greatly reduced. The particular instrument shown in figure 5 was developed at the Lewis laboratory, but the general idea is to be found in several commercial computing instruments.

The hot-wire probes are the same as described in reference 4. As discussed therein, two possible methods of wire calibration were available. Initially, the calibration procedure was to place the wire at the pipe center line and record the heat loss from the wire as the pipe mass flow was varied - the mass flow ρU being determined by independent measurements with a total-pressure probe. The second method consisted of a continuous calibration of the wire as it was operating in the pipe. Values of $\sqrt{\rho U}$ at each r distance obtained from mean velocity profile measurements with a total-pressure probe plotted against the wire heat loss recorded when the fluctuation measurements were taken results in a continuous calibration as a turbulent profile is taken. The continuous (second) method of calibration was used, since dust particles in the air stream caused discontinuous changes in the calibration curve.

The method of least squares was used to determine the slopes of the calibration curves. Because of the aforementioned discontinuous changes in wire calibration, it was often necessary to decide arbitrarily which particular set of points belonged to a given portion of the calibration curve. Cross checks between measurements (measurements at the pipe center line with Reynolds number and $\sqrt{\overline{u^2}}$ measurements evaluated from both the single and x-wire probes) were therefore employed in determining the final calibration. It is believed that the maximum error due to wire calibration was no greater than ±10 percent. A typical continuous-type calibration curve is shown in figure 6.

Some deviation from the linear relation between heat loss and the square root of mass flow was noted for the high velocities (180 ft/sec and greater).

DISCUSSION OF RESULTS

Completely describing the turbulent flow field necessitates knowing not only the time averages of the turbulent quantities appearing in the momentum and energy equations, but also all higher-order terms that might be obtained by taking higher moments of the momentum equation. At present it is neither practical nor experimentally possible to obtain all such terms; thus experimental work has been directed mainly toward measurements of only those terms appearing in the momentum equation and its first moment. The present measurements are limited almost entirely to the momentum terms. All terms of the equations of motion, simplified for fully developed pipe flow, have been measured or can be evaluated for Reynolds numbers of 25,000 and 50,000. Supplemental data at Reynolds numbers of 100,000 and 150,000 are also presented.

Mean velocity distributions. - Mean velocity profiles for the four Reynolds numbers where turbulence measurements were taken (Re = 25,000, 50,000, 100,000, and 150,000) are presented in figure 7(a). An enlarged portion of the velocity profiles near the wall is shown in figure 7(b).

The slope of the velocity profiles at the wall as predicted from dp/dx is also included in figure 7(b). Figure 8 shows a plot of the viscous shearing stress coefficient $\frac{\mu\, dU/dy}{\frac{1}{2}\rho U_c^2}$ near the wall. The existence of a nonvanishing second derivative of the velocity distribution at the wall (as indicated in fig. 8) was predicted by the analysis of Pai (ref. 8), which indicates that a nonlinear velocity distribution is consistent with the equations of motion and the boundary conditions.

Evaluation of terms in x-direction momentum equation. - The x-direction equation of motion for fully developed pipe flow may be reduced to (ref. 1)

$$\overline{uv} = \nu \frac{dU}{dr} + \frac{r}{a} U_\tau^2 \qquad (1)$$

For a major portion of the flow field $\overline{uv}$ will be the important shear term present, since only near the wall (fig. 8) is the viscous shear stress large. The distributions of $\rho\overline{uv}$, in coefficient form, across the pipe are shown in figure 9. The right side of equation (1) is plotted nondimensionally as the dashed curves of figure 9 and may be compared directly with the measured values of $\rho\overline{uv}$. Although there is considerable scatter in the $\overline{uv}$ measurements, it is evident that the data satisfy equation (1) for the range of Reynolds number investigated.

For the two higher Reynolds numbers (figs. 9(c) and (d)), it was necessary to correct the output of one of the hot wires (approximately 40 percent) so that a zero shear stress would be indicated at the center

of the pipe. (The error apparently was due to deviation of the angle of one wire, as both profiles were taken with the same probe and the same trouble was encountered.) No corrections were necessary for the probes used at the two lower Reynolds numbers. The points very close to the wall are also included, but it is evident that the presence of the wall affected the heat loss from the wires.

The measurements at a Reynolds number of 25,000 are compared with those reported in reference 1 for a 10-inch-diameter pipe, which were obtained by a method slightly different from that used in this report (see ref. 4 for method employed herein) in that the correlation coefficient $\frac{\overline{uv}}{\left(\sqrt{\overline{u^2}}\right)\left(\sqrt{\overline{v^2}}\right)}$ was measured directly, and $\overline{uv}$ was calculated from the coefficient and independent measurements of $\sqrt{\overline{u^2}}$ and $\sqrt{\overline{v^2}}$. The method of reference 1 appears to have resulted in less random scatter in the values of $\rho\overline{uv}$, but it does require a wire matching accomplished using the assumption that $\overline{uv} = 0$ at the center of the flow.

Evaluation of terms in r-direction momentum equation. - The r-direction equation of motion has in the past received little or no attention in either experimental or theoretical investigations, since for laminar shear flows the terms of this equation were found to be negligible compared with those of the x-direction equation. However, for turbulent shear flows, it is found that the turbulent contribution to the r-direction momentum results in terms as large as or larger than those appearing in the x-direction equation. It may be shown rigorously, however, that for fully developed turbulent pipe flow the x- and r-direction equations of motion are independent (ref. 1).

The r-direction equation of motion can be reduced to the form (ref. 6)

$$\overline{v^2} - \int_a^r \frac{\overline{w^2} - \overline{v^2}}{r}\,dr = \frac{p_w - p}{\rho} \tag{2}$$

Evaluation of all terms in equation (2) requires the measurement of $\overline{v^2}$ and $\overline{w^2}$ along with the variation of the static pressure across the pipe. The measurement of $\overline{v^2}$ and $\overline{w^2}$ is readily accomplished by hot wires. The static-pressure variation across the pipe is no greater than a few thousandths of an inch of water; thus no attempt was made to measure it.

The variations of $\sqrt{\overline{v^2}}$ and $\sqrt{\overline{w^2}}$ across the pipe for Re = 25,000 and Re = 50,000 are shown in figures 10(a) and (b) and 11(a) and (b), respectively. It can be seen that the two velocity components are of the same order of magnitude, with the values of $\sqrt{\overline{w^2}}$ rising to

slightly higher values as the wall is approached. The values obtained from the faired curves of figures 10 and 11 have been used to evaluate the terms on the left side of equation (2), and the resulting nondimensionalized distributions are presented in figures 12(a) and (b). Values of the right member of equation (2), obtained by subtraction of the two terms in the left member, are also plotted and show that, although the absolute magnitude of the pressure change across the pipe is small, the transverse pressure gradient is quite large, particularly near the wall. As a comparison of the orders of magnitude of the terms of the x and r momentum equations, the right side of equation (1), as presented in figure 9, has also been plotted in figure 12. The existence of large terms in the y-direction equation of motion for boundary layers has also been discussed in reference 4.

Turbulent stress tensor. - A study of the momentum distribution cannot be limited wholly to the evaluation of the time-average equations of motion, since in these equations the averaging process has eliminated some of the momentum terms present in the flow field. Reynolds' (ref. 9) investigation of turbulent flow resulted in the identification of certain virtual stress terms arising from the turbulence, which can be shown to form a turbulent stress tensor

$$\underset{\sim}{T}_T = \rho \begin{Vmatrix} \overline{u^2} & \overline{uv} & \overline{uw} \\ \overline{vu} & \overline{v^2} & \overline{vw} \\ \overline{wu} & \overline{wv} & \overline{w^2} \end{Vmatrix} \tag{3}$$

For the fully developed turbulent pipe flow it is possible to show that

$$\overline{wv} = \overline{vw} = \overline{wu} = \overline{uw} = 0 \quad \text{and} \quad \overline{uv} = \overline{vu}$$

so that only four of the terms are independent.

The only term appearing in the stress tensor which does not also appear in some form in the equations of motion is $\rho\overline{u^2}$. The measurements of $\sqrt{\overline{u^2}}$ for the four Reynolds numbers investigated are presented in figure 13. It may be seen that the values of $\overline{u^2}$ are by far the largest terms in the stress tensor (eq. (3)), with magnitudes as great as four times that of any of the other terms for the region close to the wall. Near the center the value of $\overline{u^2}$ approaches that of $\overline{v^2}$, so that the conditions of isotropy are nearly satisfied at the center of the pipe.

A second factor of importance in regard to the turbulent stress tensor is the direction along which the maximum stress acts. For the

turbulent stress tensor, the angle β between the principal axis of the tensor and the direction of mean flow is given by the equation (ref. 10)

$$\tan 2\beta = \frac{2\overline{uv}}{\overline{u^2} - \overline{v^2}} \tag{4}$$

The values calculated for β are shown in figure 14. The evaluation of β near the center of the pipe is not accurate because equation (4) is extremely sensitive to the measured values in this region since $\overline{u^2} \rightarrow \overline{v^2}$ and $\overline{uv} \rightarrow 0$ at $r = 0$. As the wall is approached, the angle β decreases so that the direction of principal stress is alined nearly parallel to the flow and the wall.

Reynolds number effects. - The effect of Reynolds number on turbulent intensity has been determined from experimental measurements of the turbulent intensities at the pipe center. Figures 15 and 16 show the variation of the two turbulent velocity components $\sqrt{\overline{u^2}}$ and $\sqrt{\overline{v^2}}$ along the pipe center with Reynolds number. The points are also compared with data from references 1, 2, and 11. Results in figure 15 indicate that the variation of the longitudinal component with Re can be considered universal within the limits of experimental accuracy. It is noted in reference 12 that for a fully developed channel flow the intensity at the center was independent of any upstream turbulence, thus showing that the turbulence has reached a statistical equilibrium state which will not change unless the symmetry of the flow is disturbed. The following empirical equation is found to fit the data of figure 15:

$$\left(\frac{\sqrt{\overline{u^2}}}{U_c}\right)_{\text{at } r=0} = 0.144\ \mathrm{Re}^{-0.146} \tag{5}$$

A summary of the variation of the longitudinal turbulent intensity distribution is shown in figure 17. Figure 18 shows the $\sqrt{\overline{u^2}}$ profile presented in reference 1 for Re = 250,000 compared with a distribution for Re = 200,000 measured in the 4-inch pipe.

Comparison of constant-current and constant-temperature hot-wire anemometer systems. - A direct comparison of measurements made using the two types of hot-wire anemometer systems employed is shown in figure 15. The feasibility of using the constant-temperature system for measurement of turbulence intensities encountered in turbulent shear flows has been questioned (ref. 3), since the noise level of the system was considered too high. However, for the turbulence levels encountered in the pipe, constant-temperature measurements agree with constant-current measurements within the range of experimental accuracy. All distribution

measurements across the pipe reported herein were taken with the constant-temperature instruments, since only a fraction of the time per measurement was required as compared with that needed in constant-current measurements. Since the measurements reported by Laufer (ref. 1) were performed with a constant-current system, the comparison of profiles (figs. 9(a), 10(a), 11(a), and 13(a)) also offers a check of the agreement between the two systems.

Comparison of pipe and channel flow. - A brief comparison between the flow in a pipe and that in a channel was made. Measurements of the $\sqrt{\overline{u^2}}$ distribution in a channel for Re = 61,000 reported in reference 2 are shown in figure 19. The distribution of $\sqrt{\overline{u^2}}$ measured for the same Reynolds number in the 4-inch pipe is also included in figure 19. It may be seen that the distributions for the pipe and the channel are similar.

Spectrum measurements. - The spectra of the longitudinal turbulent intensity for Re = 25,000 at several r-distances obtained by use of a harmonic wave analyzer are shown in figure 20. The function F(n) was defined as

$$F(n) = \frac{d\left(\overline{u_n^2}\right)}{\overline{u^2}\, dn} \tag{9}$$

where $d\left(\overline{u_n^2}\right)$ is the contribution to $\overline{u^2}$ from frequencies $n - \frac{dn}{2}$ and $n + \frac{dn}{2}$, and dn is the effective band width of the measuring analyzer (4.4 cps). Figure 20 shows a redistribution in the high-frequency range for the spectrum distribution very near the wall.

CONCLUDING REMARKS

Analysis of the measured momentum terms in fully developed turbulent pipe flow indicates that the balance of the longitudinal-direction momentum terms as predicted from the Reynolds equation of motion can be experimentally verified. Evaluation of the terms in the radial-direction momentum balance shows the existence of a pressure gradient across the pipe. The terms of the r-direction momentum equation for turbulent pipe flow are comparable in magnitude with those of the x-direction equation; however, the two equations are independent.

Evaluation of the turbulent stress tensor shows the mean square longitudinal velocity to be by far the largest term near the wall, with

the other three terms being of roughly equal magnitude. The calculation of the angle between the principal axis of the stress tensor and the x-direction shows the axis to be oriented nearly parallel to the wall in the region near the wall.

A study of the Reynolds number effects on the longitudinal turbulent intensity at the center of the pipe indicates that the intensities are of a universal nature. Comparison of $\sqrt{\overline{u^2}}$ and $\sqrt{\overline{v^2}}$ at the center indicates the flow to be nearly isotropic.

The longitudinal turbulent intensity at the center of the pipe could be represented by the empirical relation

$$\frac{\sqrt{\overline{u^2}}}{U_c} = 0.144\ Re^{-0.146}$$

where $\sqrt{\overline{u^2}}$ is the root mean square of the longitudinal turbulent velocity, U_c is the mean velocity at the center of the pipe, and Re is the Reynolds number.

Direct comparison of the constant-current and constant-temperature systems of hot-wire measurements of turbulent quantities showed agreement within the limits of experimental accuracy. The constant-temperature measurements at Re = 25,000 are found to agree within the limits of experimental accuracy with the measurements presented by Laufer for the same Reynolds number.

Lewis Flight Propulsion Laboratory
National Advisory Committee for Aeronautics
Cleveland, Ohio, August 27, 1954

APPENDIX - SYMBOLS

a	radius of pipe
h	channel half-width
i	mean current of hot wire
p	mean static pressure
p_w	mean static pressure at wall
R	operating resistance of hot wire
R_a	resistance of hot wire at reference condition
Re	Reynolds number based on channel half-width or pipe radius and velocity at center of flow, $\rho U_c a/\mu$ or $\rho U_c h/\mu$
r	radial distance from pipe center
r'	$(a - r)$
$\underset{=}{T}_T$	turbulent stress tensor
U	mean longitudinal velocity
U_c	mean longitudinal velocity at center of pipe or channel
U_τ	shear stress velocity, $\sqrt{\tau_w/\rho}$
u,v,w	longitudinal, radial, and tangential components of turbulent velocity
$\overline{uv}$	Reynolds turbulent shear stress in xr-plane
$\overline{uw}$	Reynolds turbulent shear stress in x-tangential plane
$\overline{vw}$	Reynolds turbulent shear stress in r-tangential plane
x	direction of mean flow
β	angle between principal axis of turbulent stress tensor and direction of mean flow
μ	viscosity of air
ν	kinematic viscosity of air

ρ density of air

τ_w shearing stress at wall

REFERENCES

1. Laufer, John: The Structure of Turbulence in Fully Developed Pipe Flow. NACA TN 2954, 1953.

2. Laufer, John: Investigation of Turbulent Flow in a Two-Dimensional Channel. NACA Rep. 1053, 1951. (Supersedes NACA TN 2123.)

3. Kovasznay, Leslie S. G.: Simple Analysis of the Constant Temperature Feedback Hot-Wire Anemometer. Aero./JHU CM-478, Dept. Aero., Johns Hopkins Univ., June 1, 1948. (NOrd-8036, T.O. JHB-6.)

4. Sandborn, Virgil A., and Slogar, Raymond J.: Study of the Momentum Distribution of Turbulent Boundary Layers in Adverse Pressure Gradients. NACA TN 3264.

5. Goldstein, Sidney: Modern Developments in Fluid Dynamics. vol. I. Clarendon Press, 1938, p. 255.

6. Schubauer, G. B., and Klebanoff, P. S.: Theory and Application of Hot-Wire Instruments in the Investigation of Turbulent Boundary Layers. NACA WR W-86, 1946. (Supersedes NACA ACR 5K27.)

7. Laurence, James C., and Landes, L. Gene: Auxiliary Equipment and Techniques for Adapting the Constant-Temperature Hot-Wire Anemometer to Specific Problems in Air-Flow Measurements. NACA TN 2843, 1952.

8. Pai, S. I.: On Turbulent Flow in Circular Pipe. Jour. Franklin Inst., vol. 256, no. 4, Oct. 1953, pp. 337-352.

9. Reynolds, Osborne: On the Dynamical Theory of Incompressible Viscous Fluids and the Determination of the Criterion. Phil. Trans. Roy. Soc. (London), ser. A, vol. 186, 1895, pp. 123-164.

10. Dryden, Hugh L.: Some Recent Contributions to the Study of Transition and Turbulent Boundary Layers. NACA TN 1168, 1947.

11. Newman, B. G., and Leary, B. G.: The Measurement of the Reynolds Stresses in a Circular Pipe as a Means of Testing a Hot-Wire Anemometer. Rep. A.72, Aero. Res. Lab., Commonwealth of Australia, Nov. 1950.

12. Wattendorf, F. L., and Kuethe, A. M.: Investigation of Turbulent Flow by Means of the Hot-Wire Anemometer. Phys., vol. 5, no. 6, June 1934, pp. 153-164.

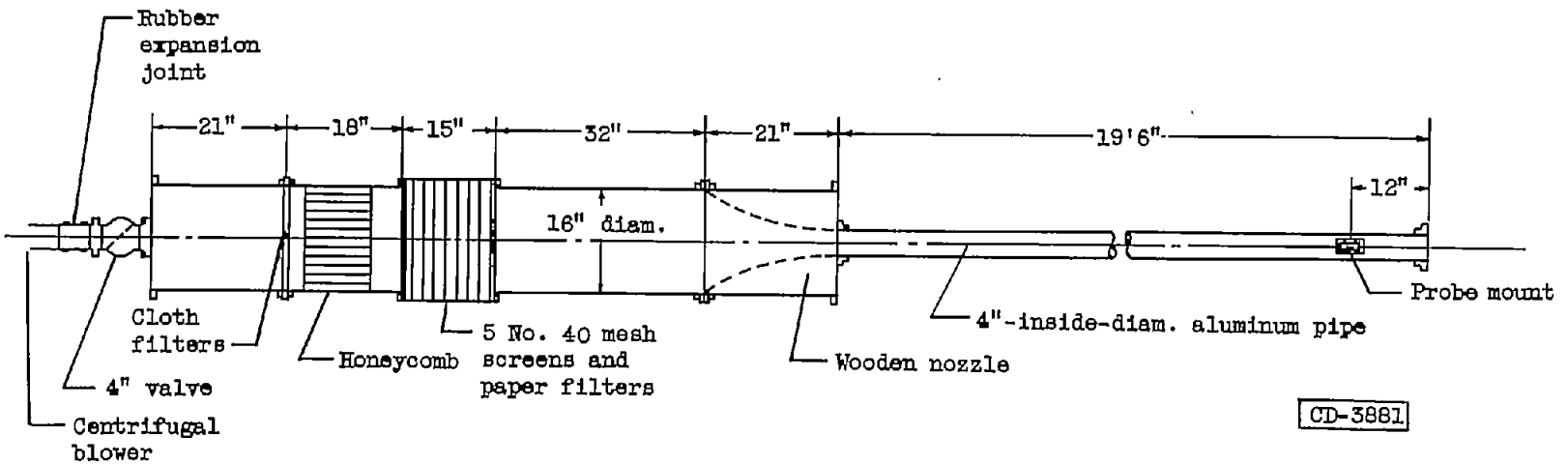

Figure 1. - Schematic diagram of 4-inch-diameter pipe.

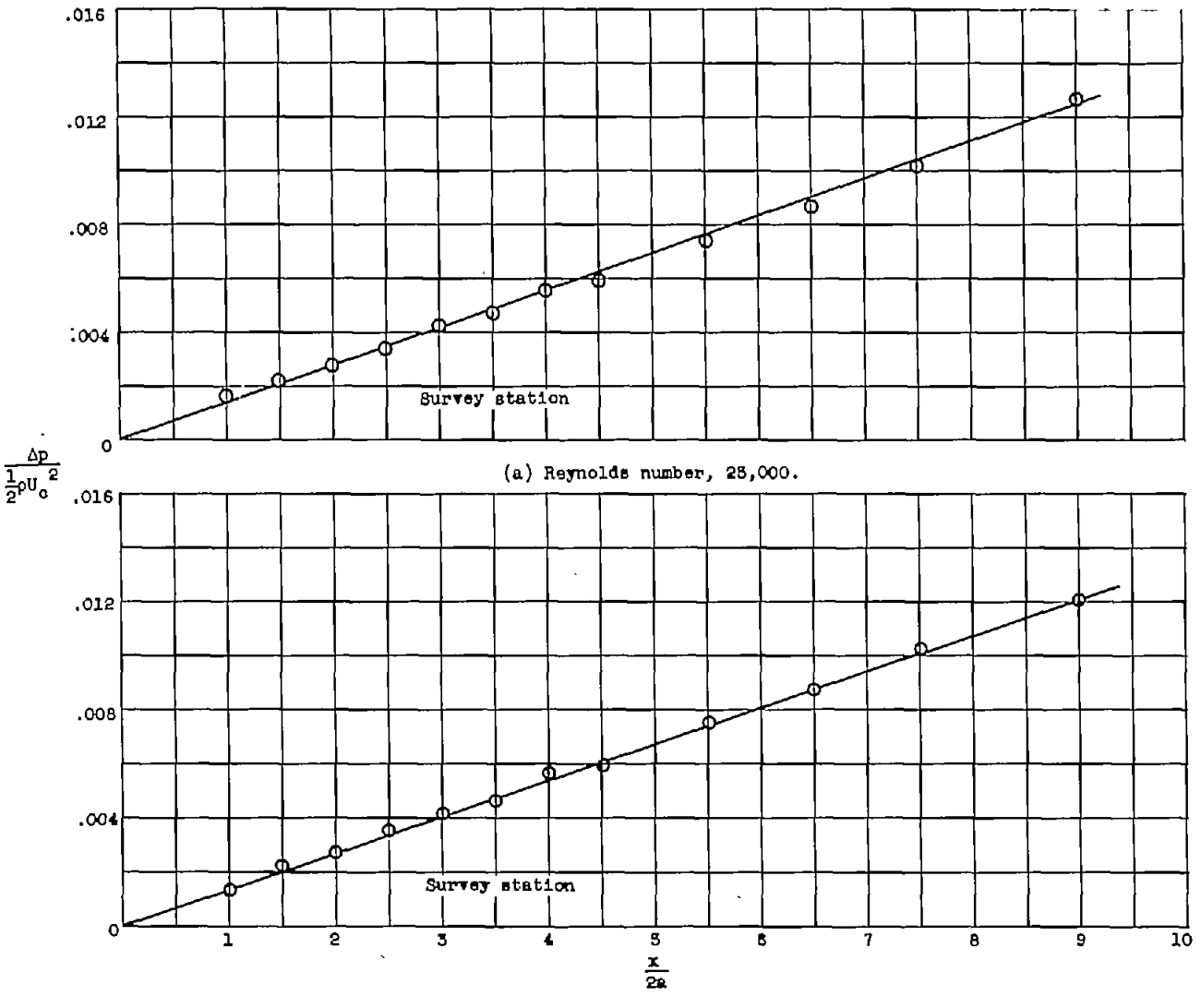

(a) Reynolds number, 25,000.

(b) Reynolds number, 50,000.

Figure 2. - Static-pressure distribution along pipe wall.

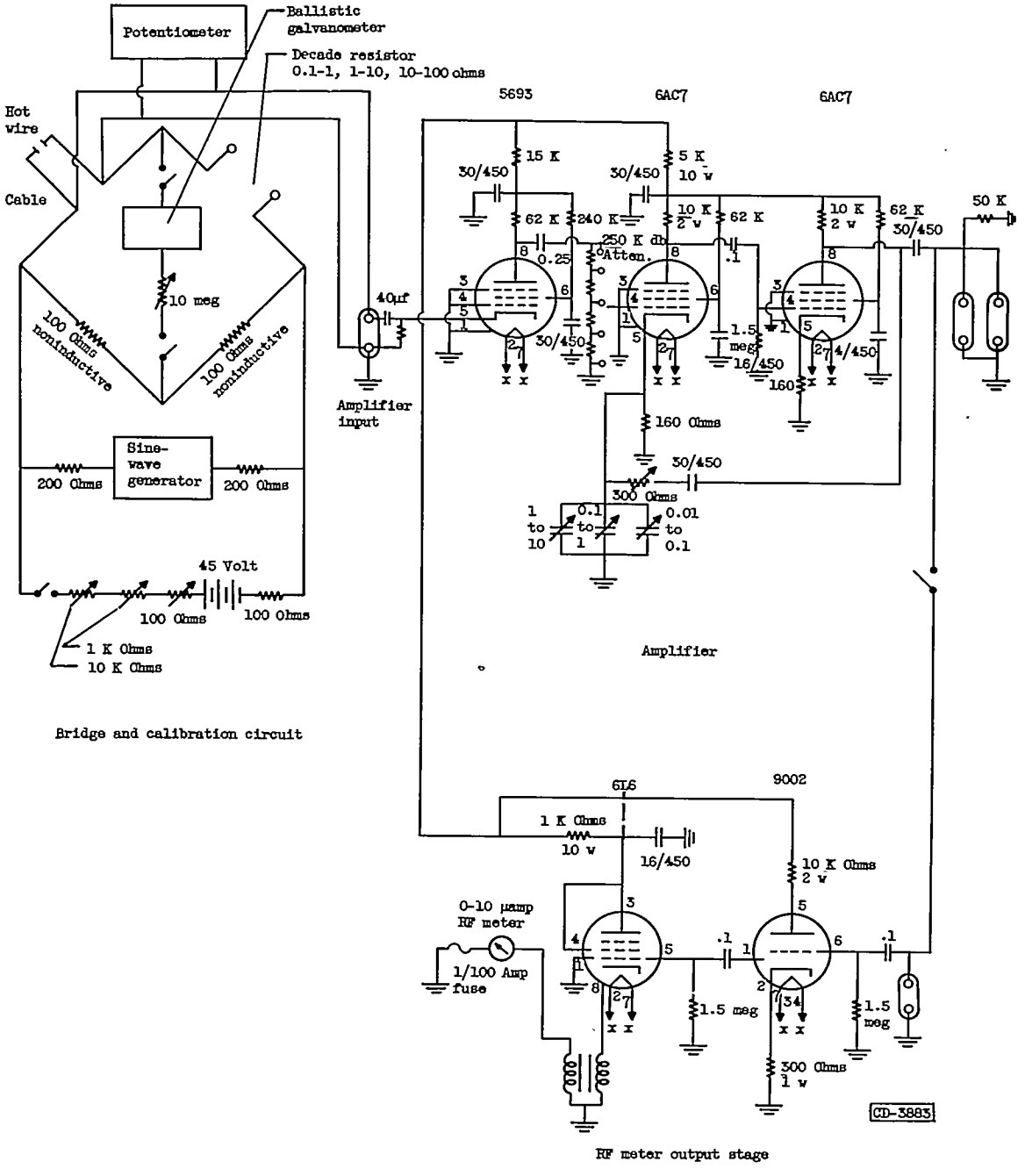

Figure 3. - Constant-current hot-wire anemometer circuit.

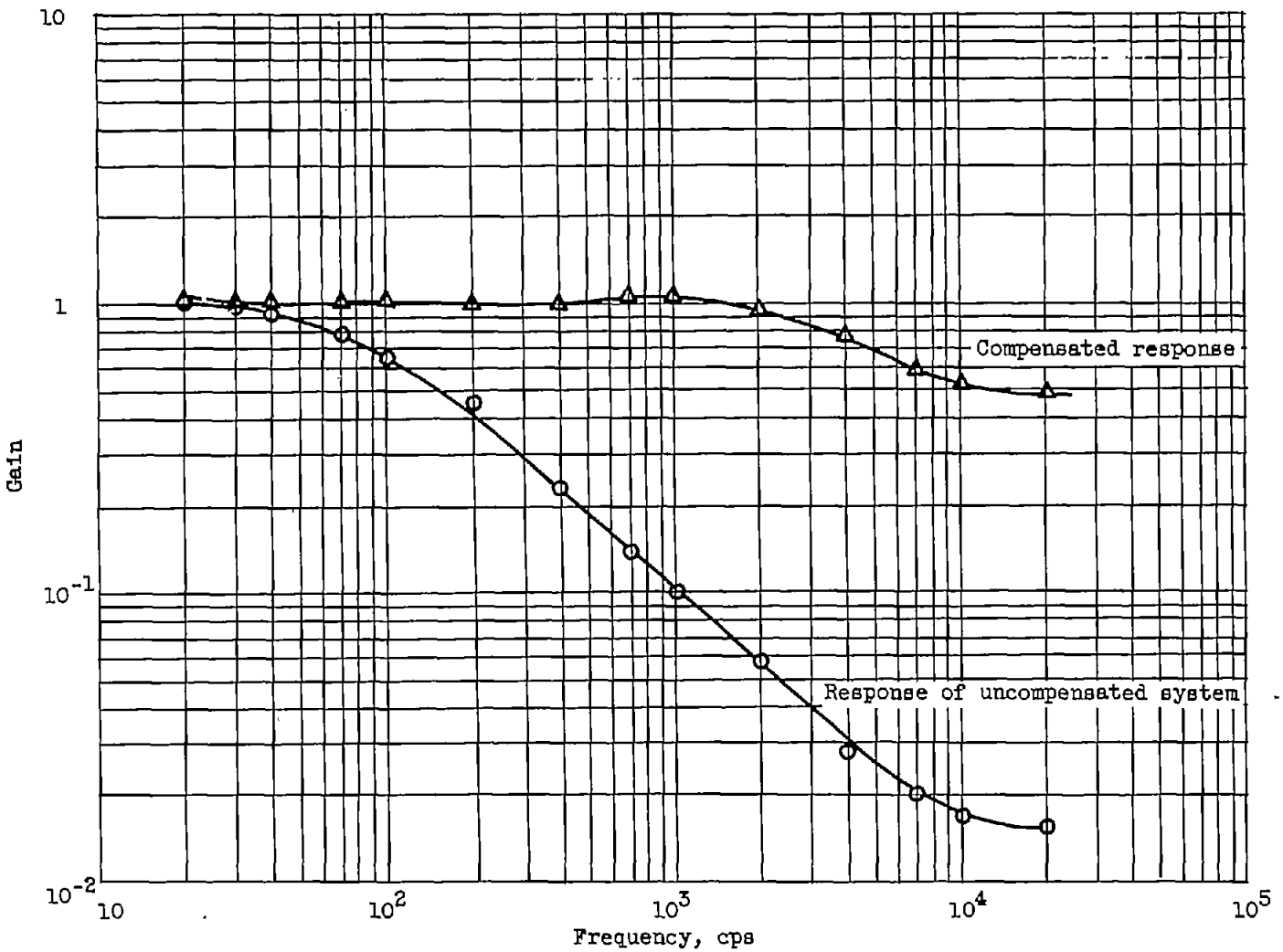

Figure 4. - Frequency response of uncompensated and compensated constant-current hot-wire anemometer system. (Gain is ratio of rms voltages, arbitrary units plotted.)

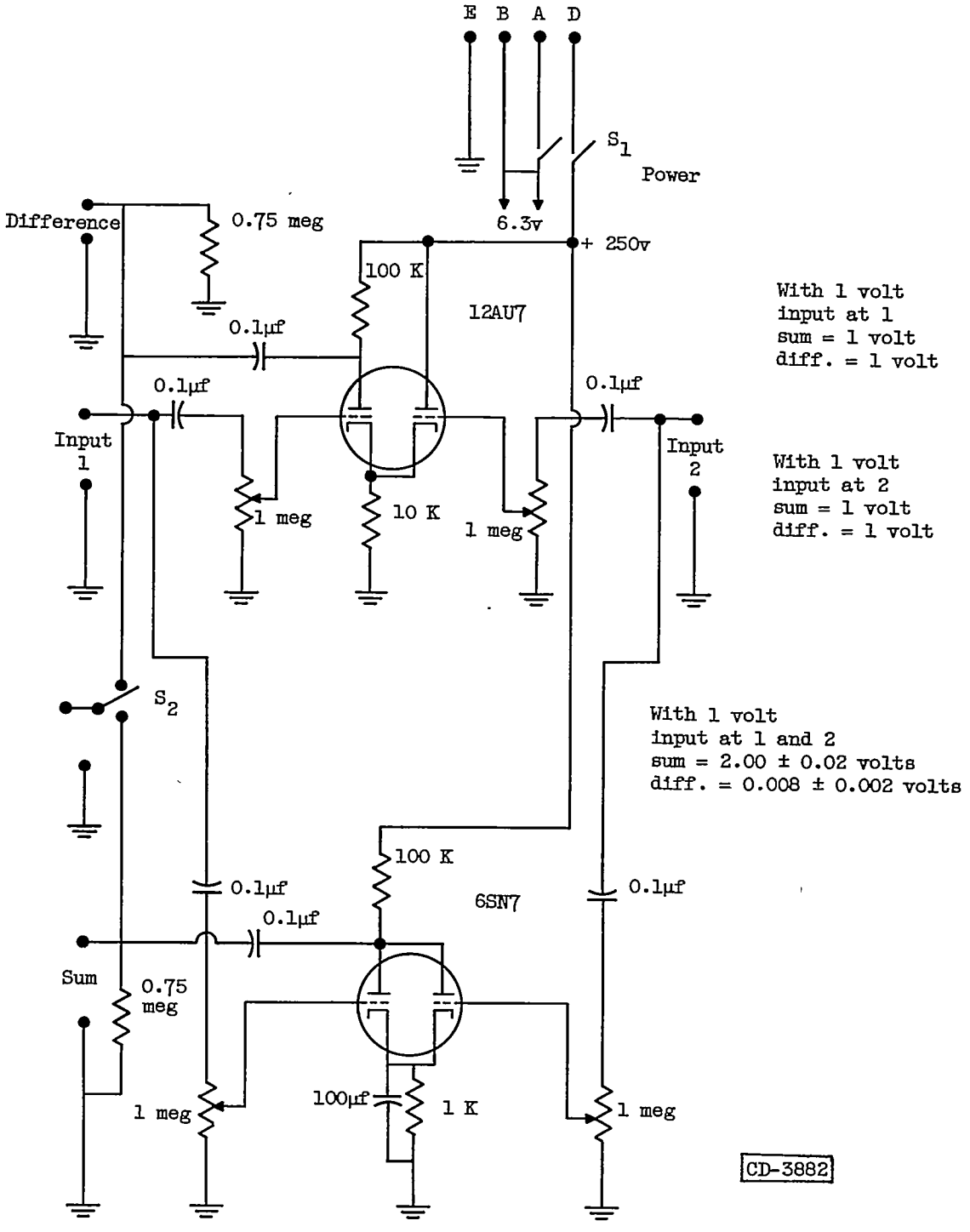

Figure 5. - Wiring diagram of sum and difference circuit.

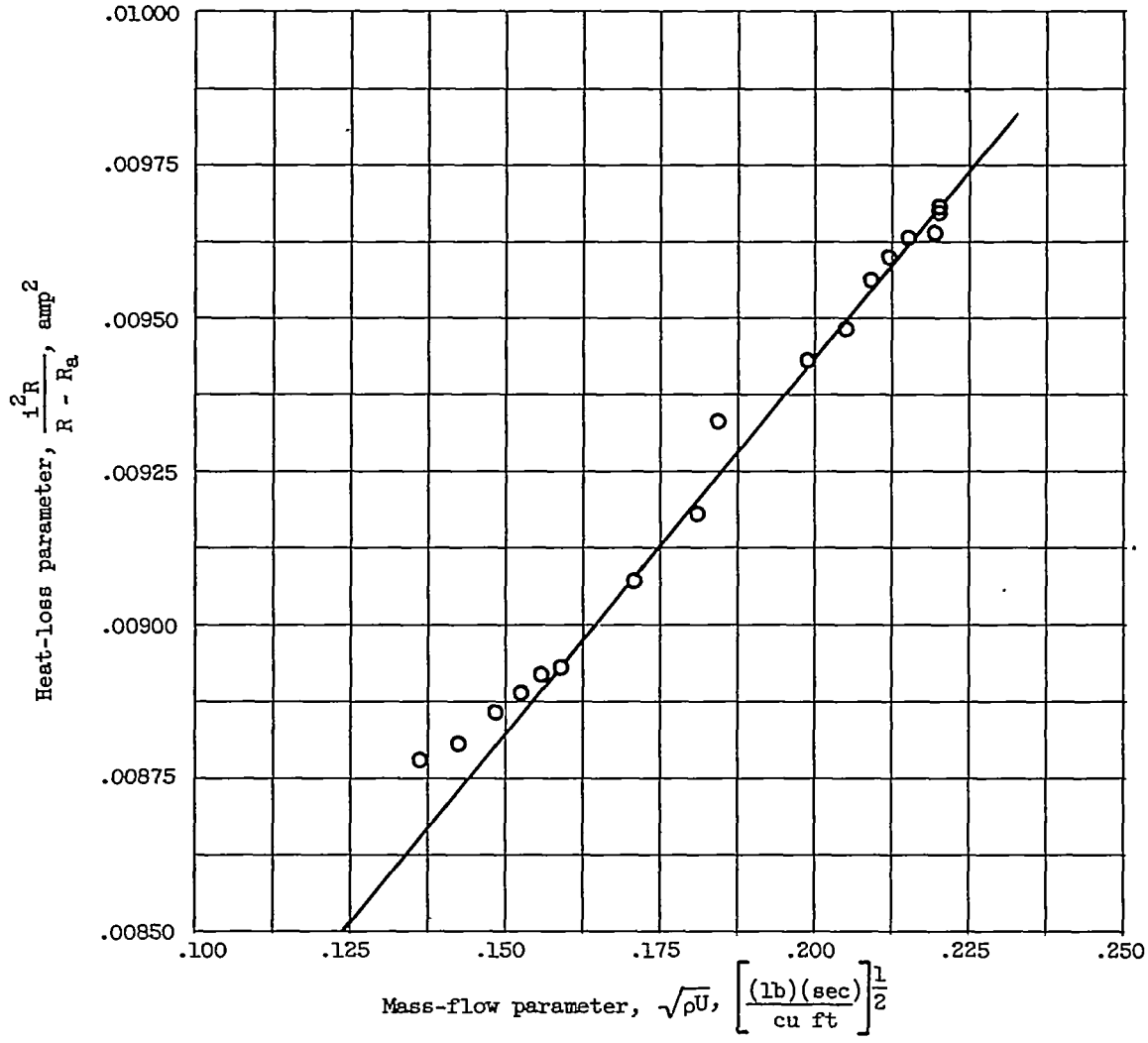

Figure 6. - Hot-wire calibration curve. Constant-temperature operation; slope calculated by method of least squares neglecting points near wall.

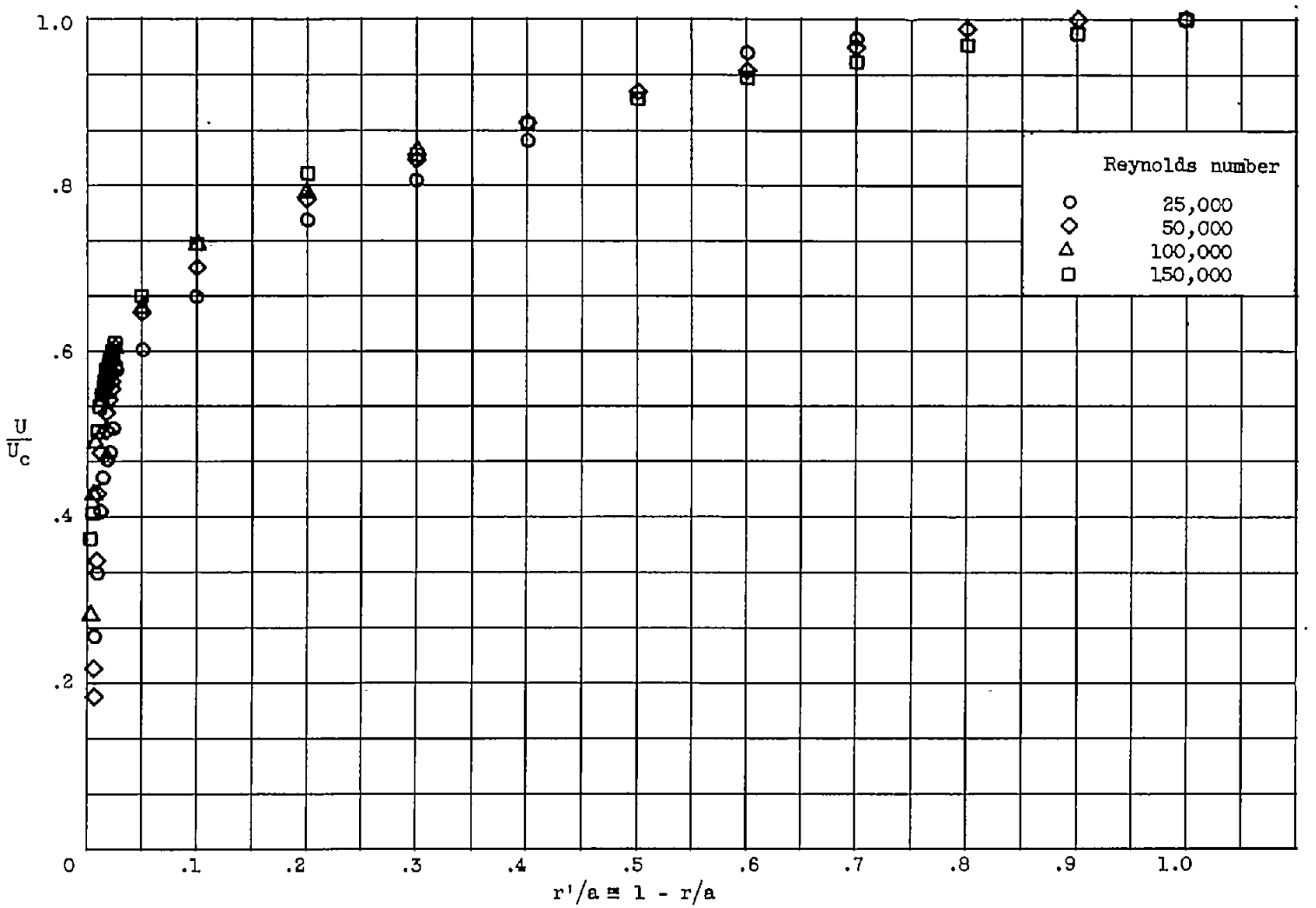

(a) Mean velocity distribution across pipe.

Figure 7. - Mean velocity profiles.

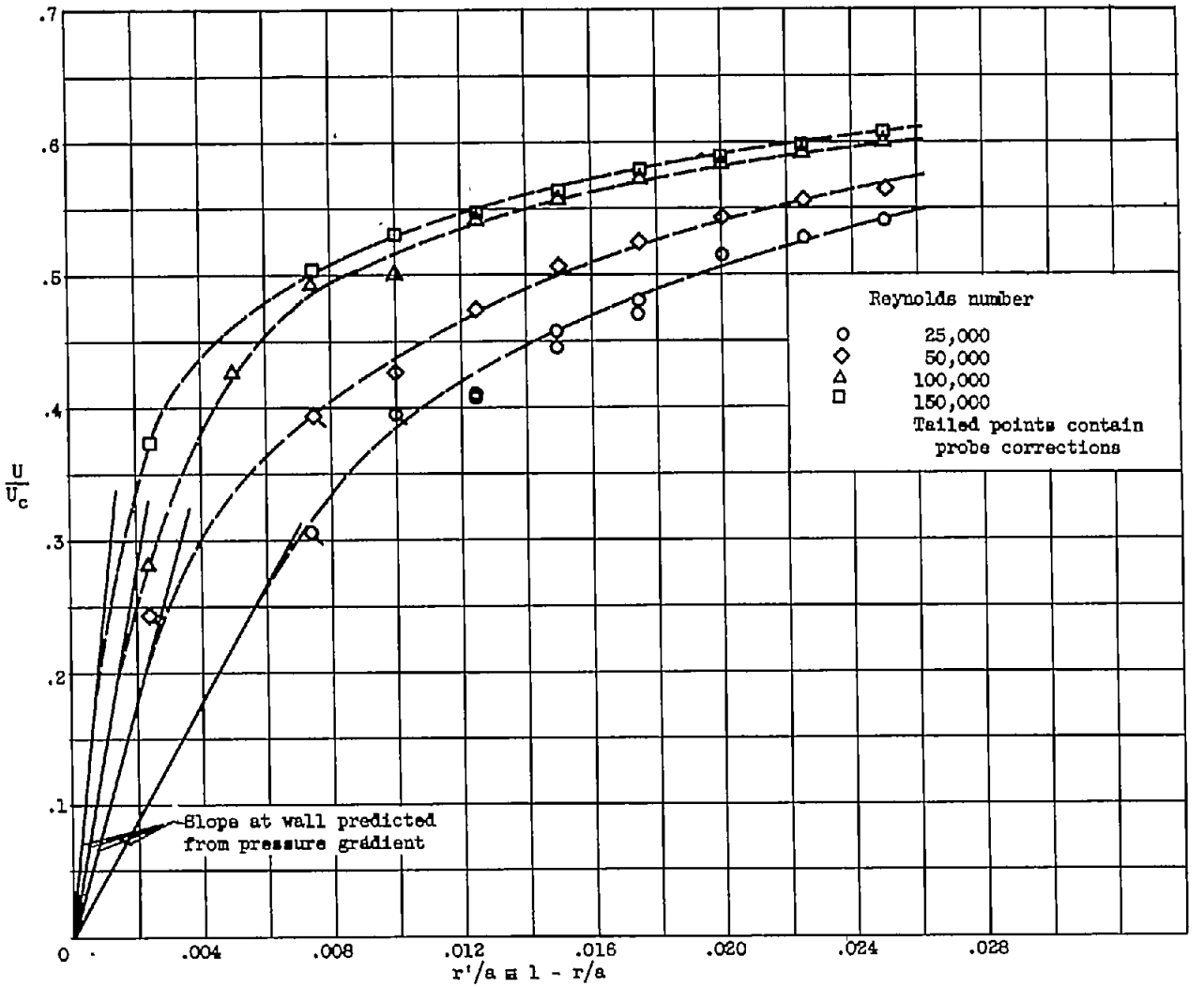

(b) Mean velocity distribution near wall.

Figure 7. - Concluded. Mean velocity profiles.

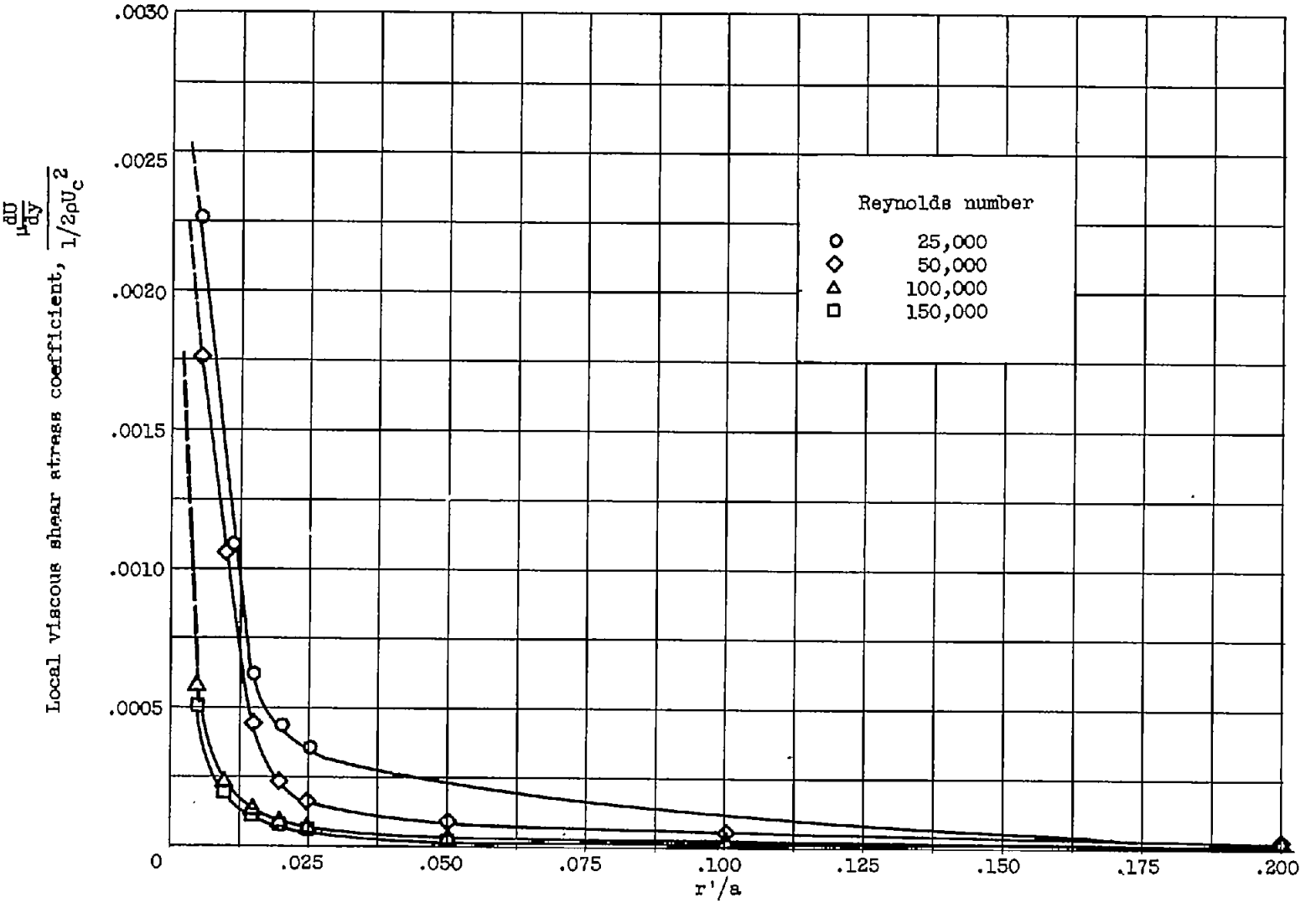

Figure 8. - Variation of viscous shear stress near wall.

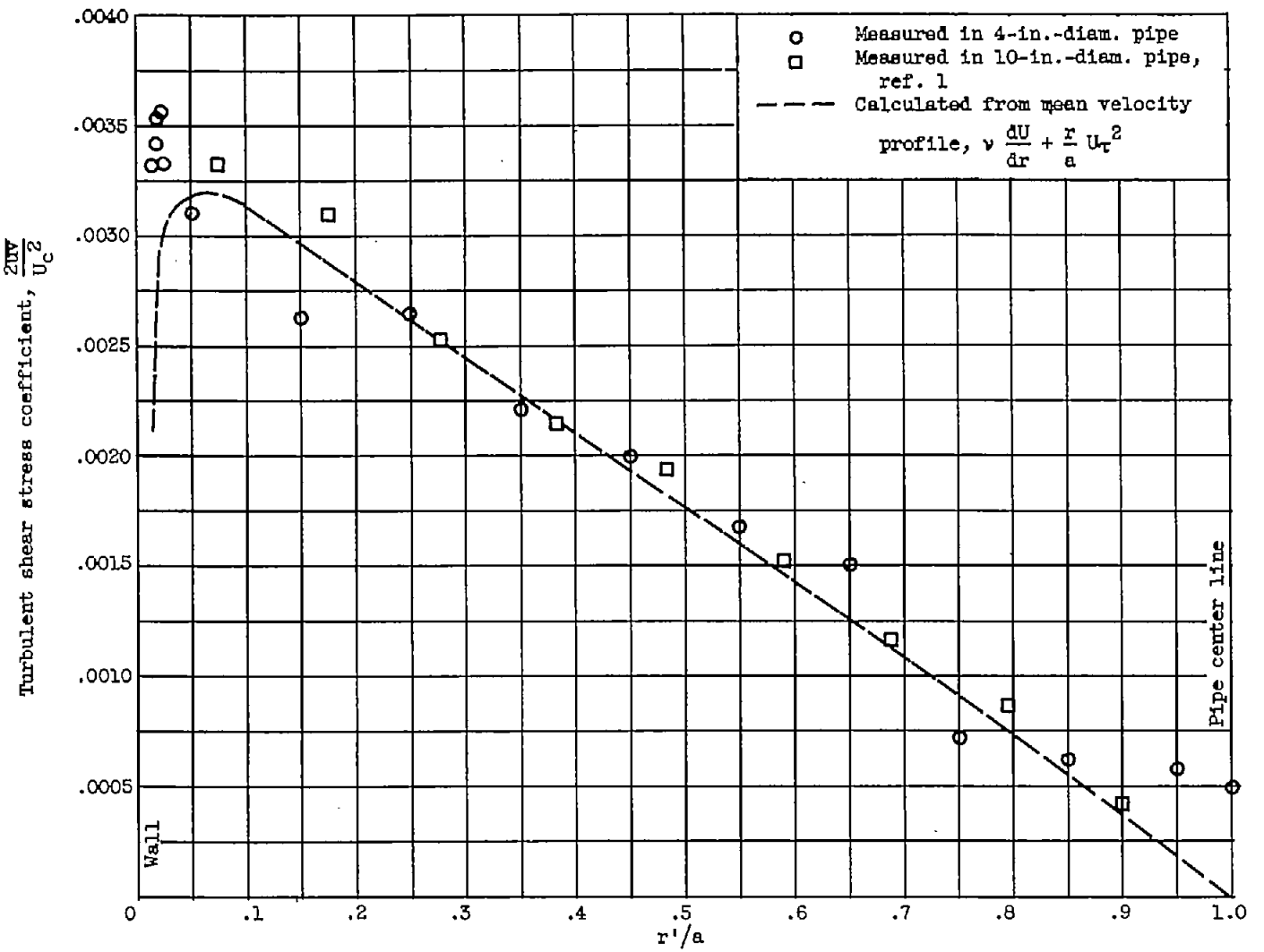

(a) Reynolds number, 25,000.

Figure 9. - Distribution of turbulent shear stress coefficient across pipe.

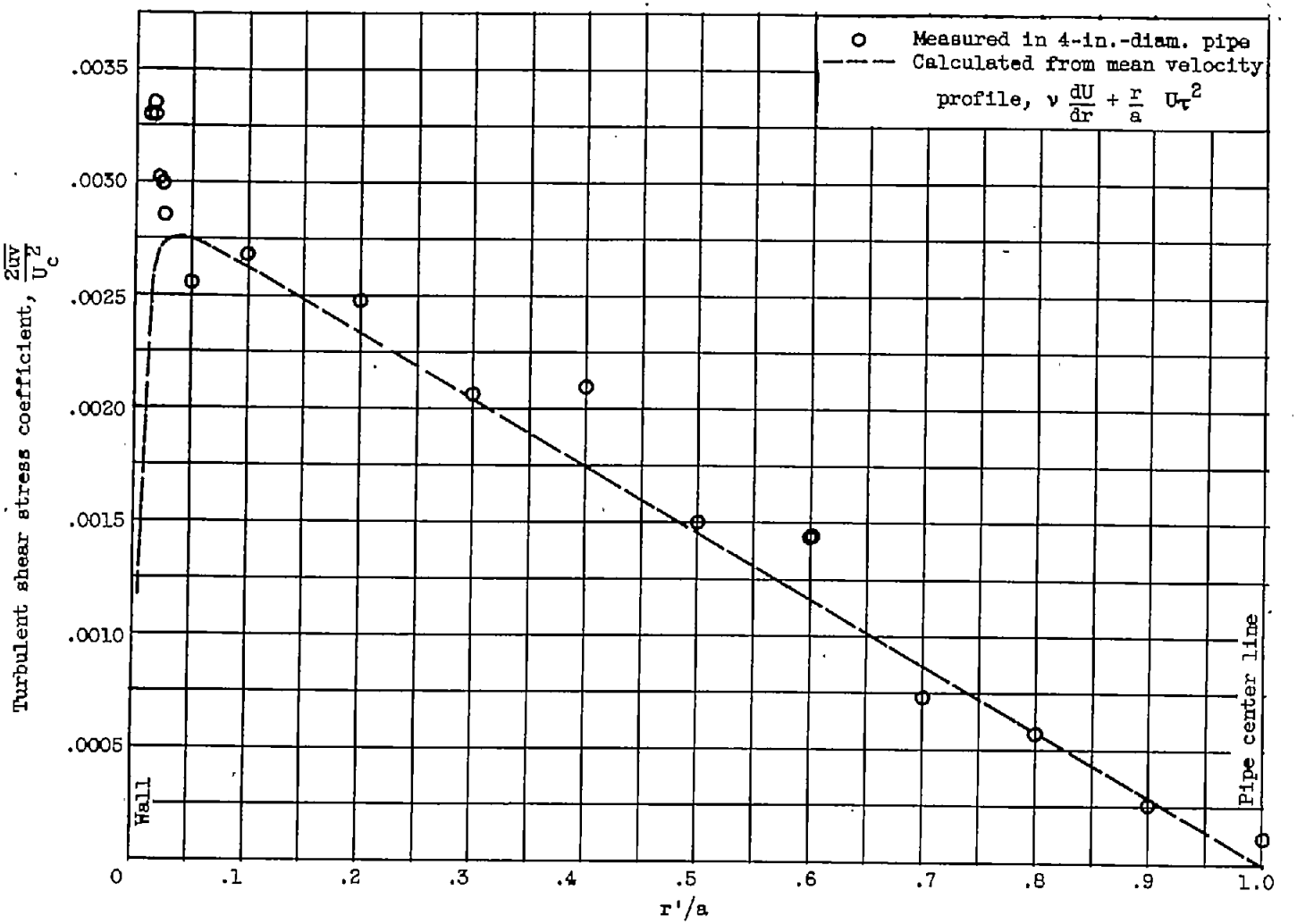

(b) Reynolds number, 50,000.

Figure 9. - Continued. Distribution of turbulent shear stress coefficient across pipe.

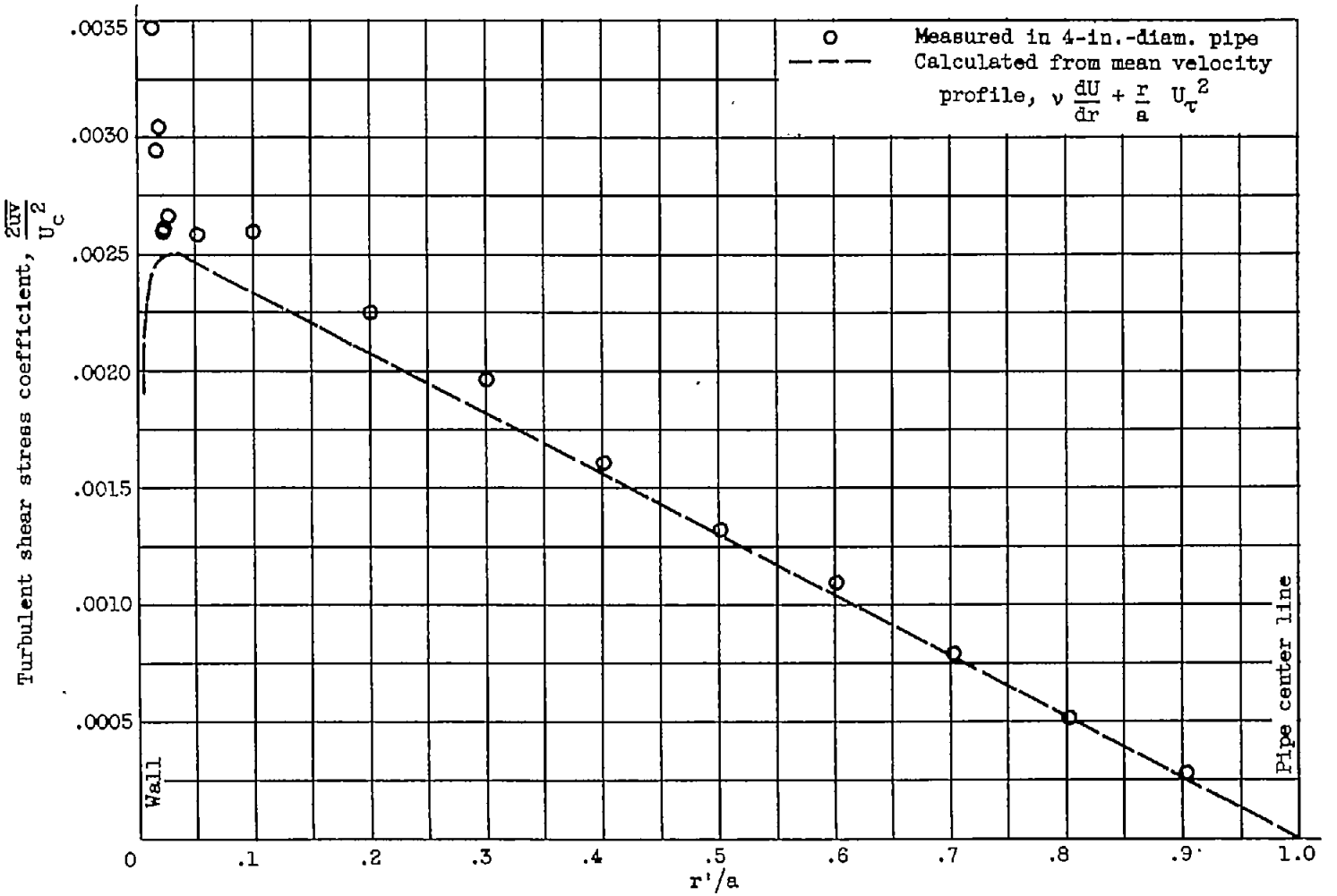

(c) Reynolds number, 100,000.

Figure 9. - Continued. Distribution of turbulent shear stress coefficient across pipe.

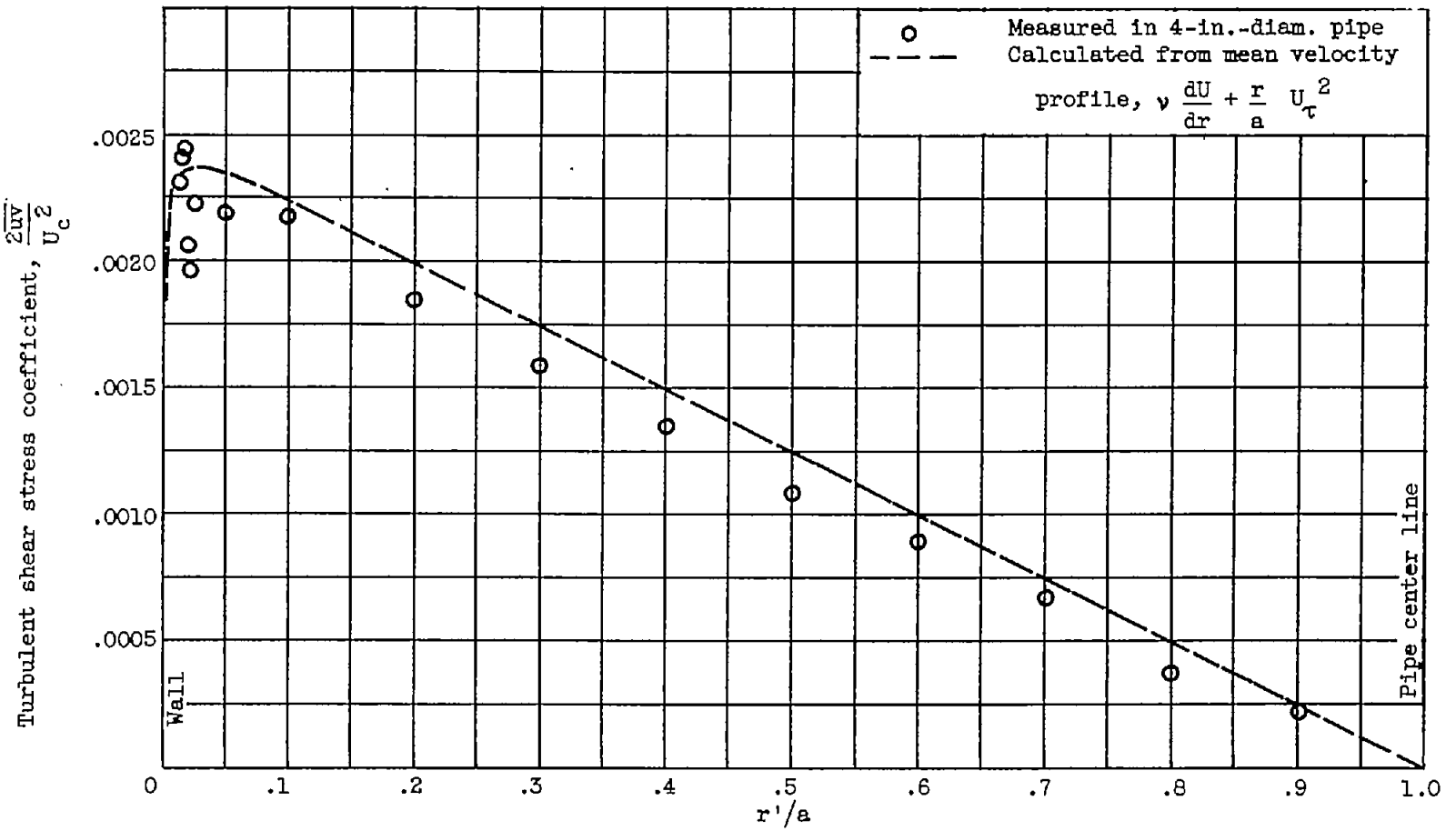

(d) Reynolds number, 150,000.

Figure 9. - Concluded. Distribution of turbulent shear stress coefficient across pipe.

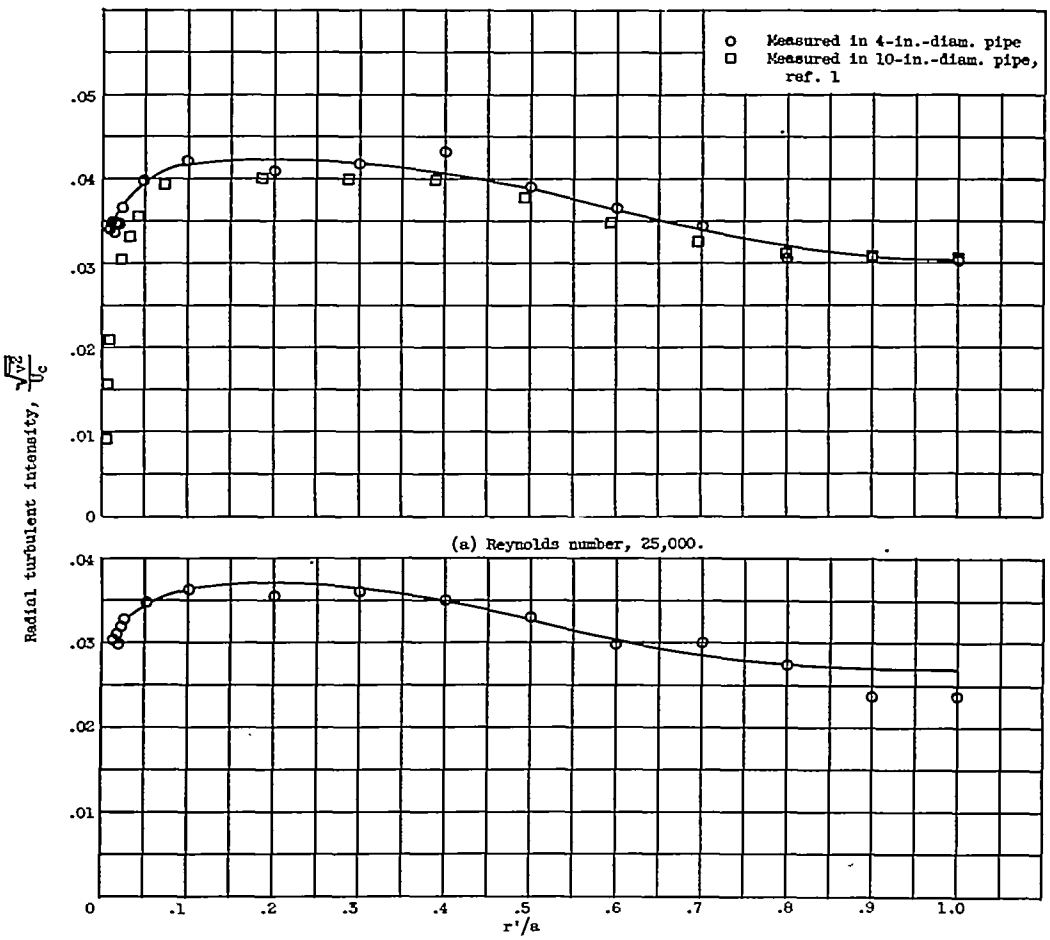

(a) Reynolds number, 25,000.

(b) Reynolds number, 50,000.

Figure 10. - Radial turbulent intensity distribution across pipe.

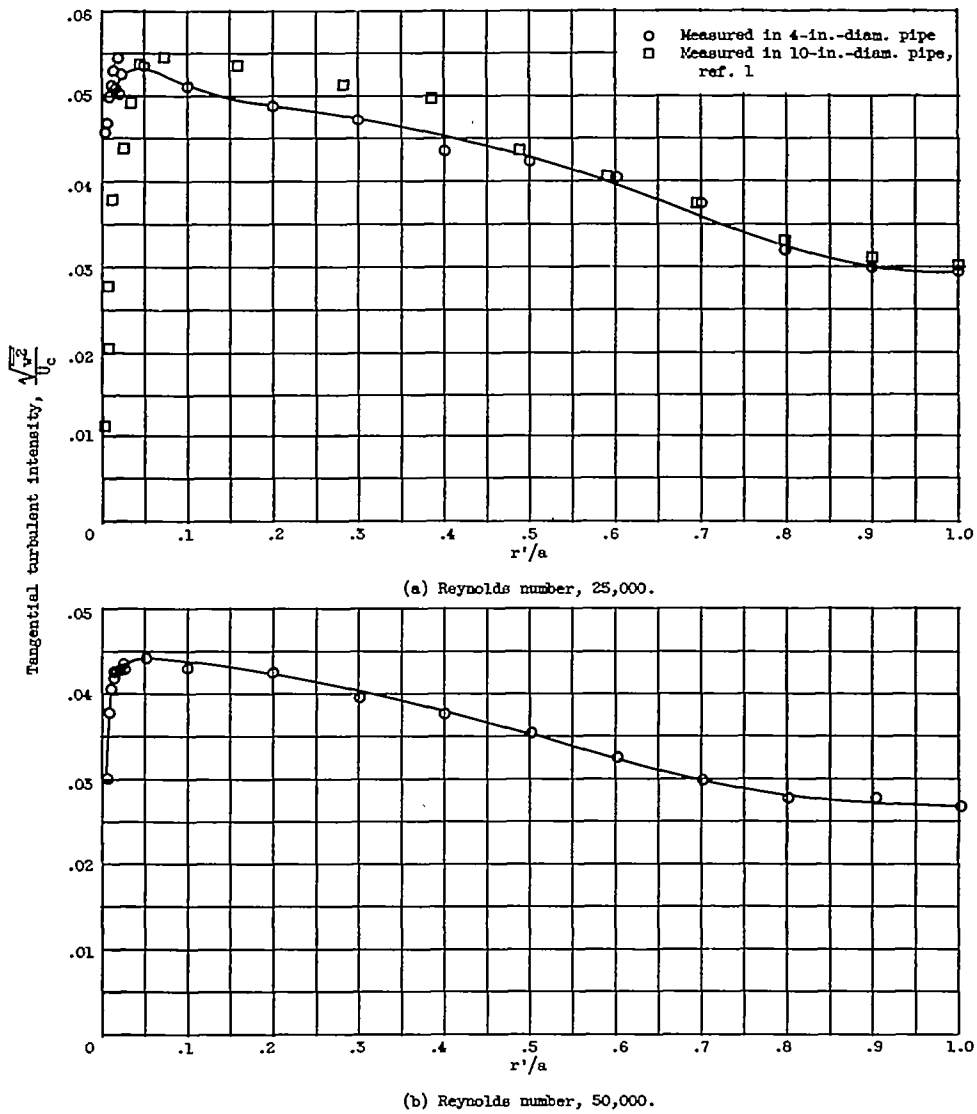

(a) Reynolds number, 25,000.

(b) Reynolds number, 50,000.

Figure 11. - Tangential turbulent intensity distribution across pipe.

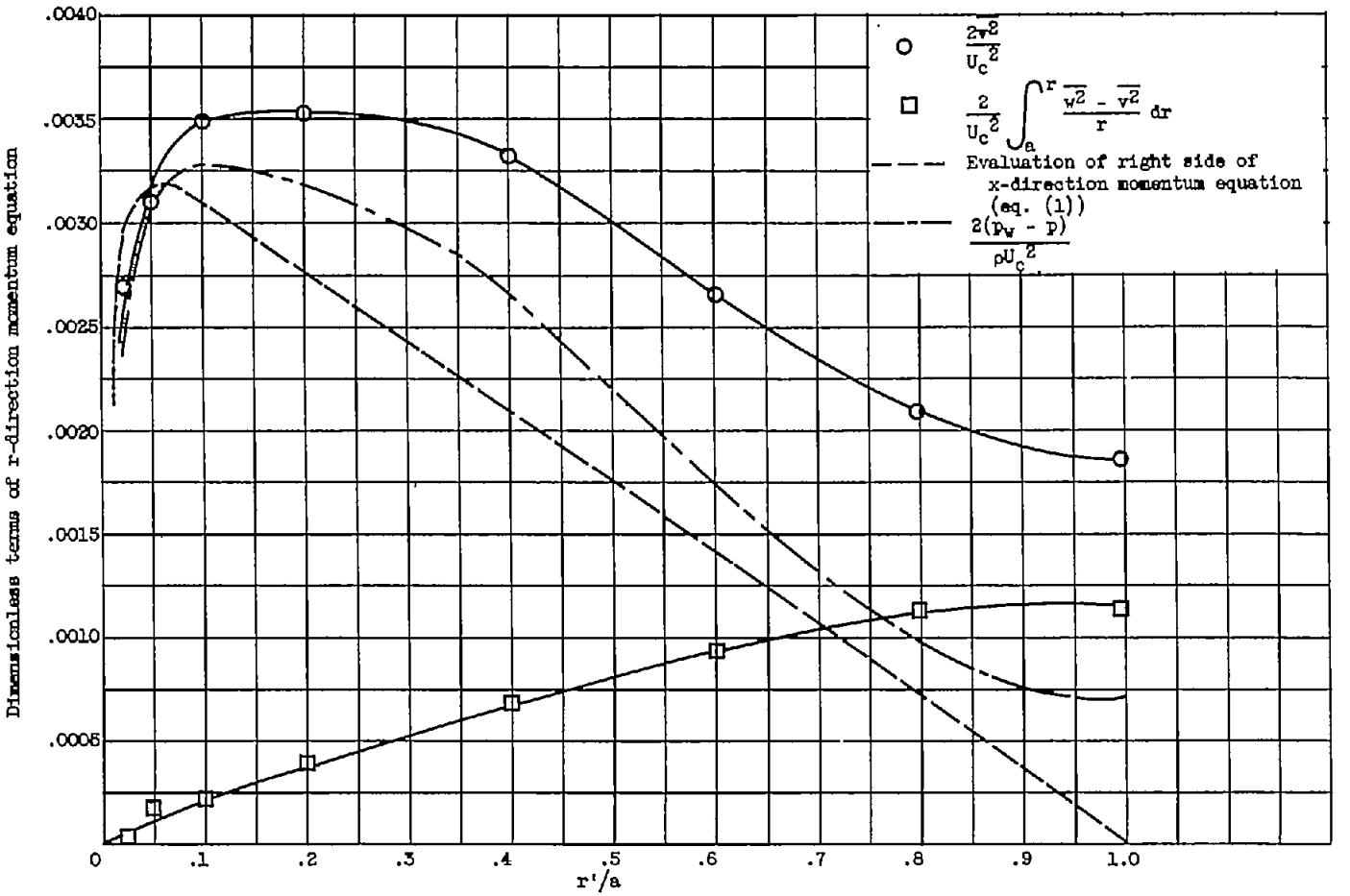

(a) Reynolds number, 25,000.

Figure 12. - Variation of terms in r-direction momentum equation.

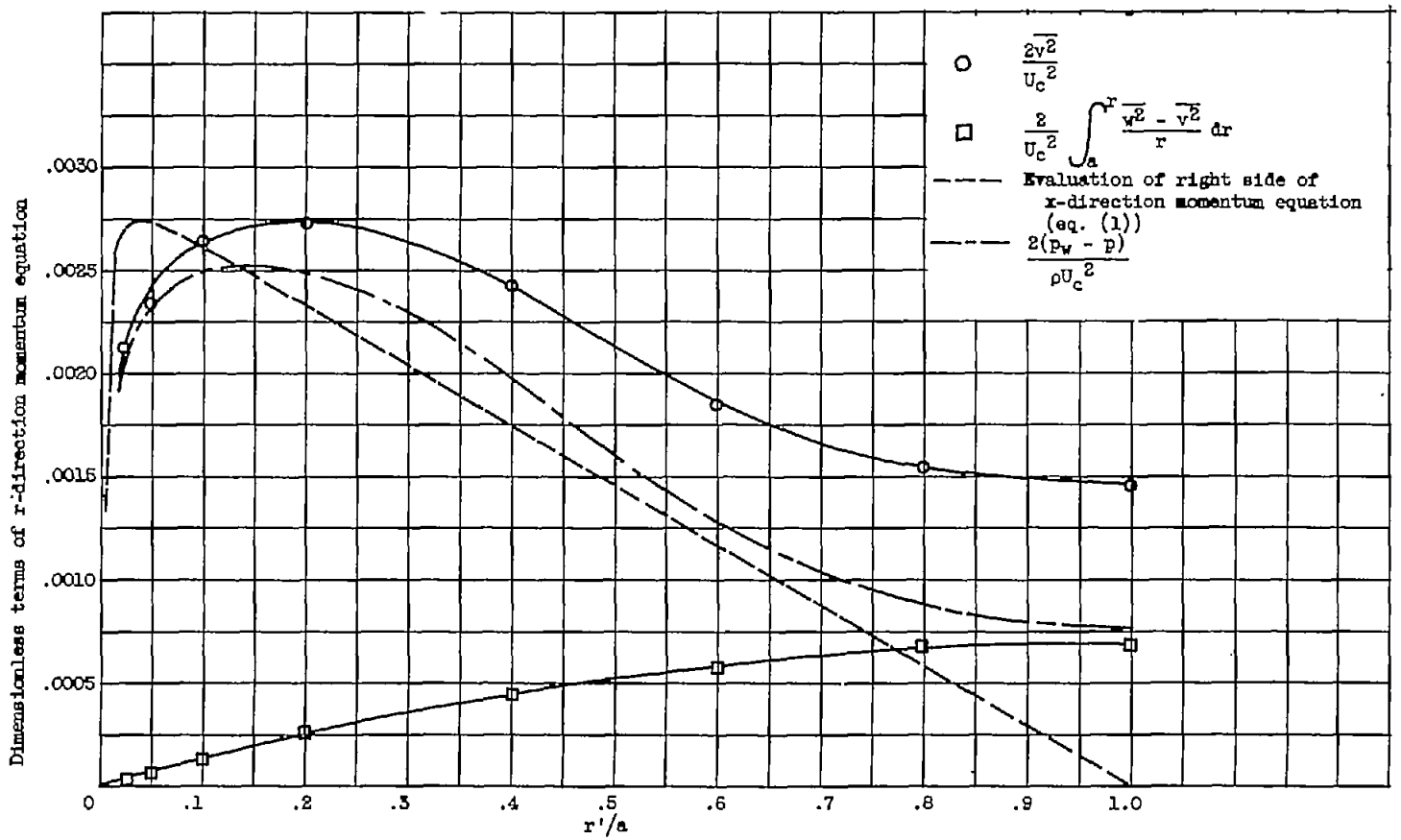

(b) Reynolds number, 50,000.

Figure 12. - Concluded. Variation of terms in r-direction momentum equation.

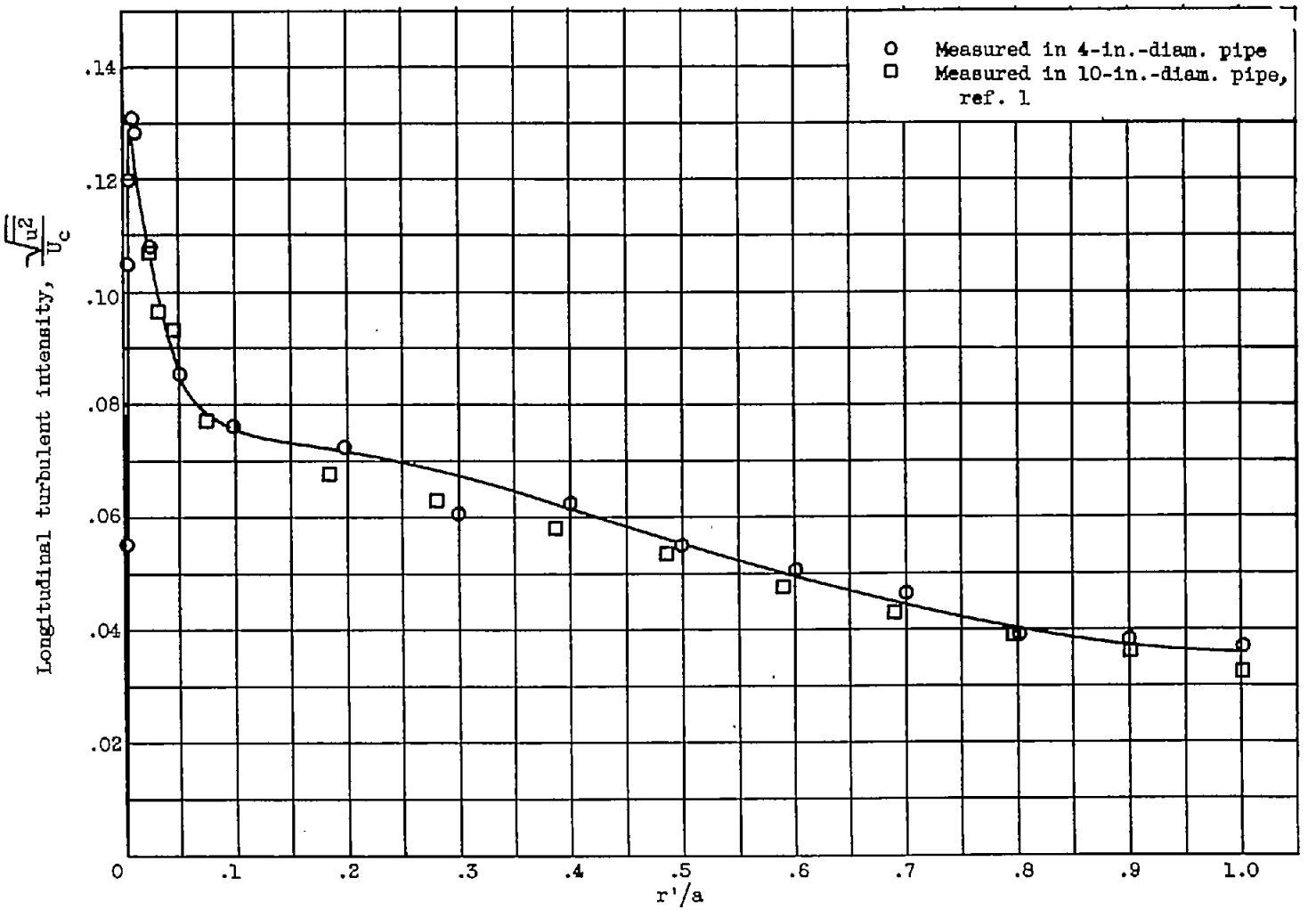

(a) Reynolds number, 25,000.

Figure 13. - Longitudinal turbulent intensity distribution across pipe.

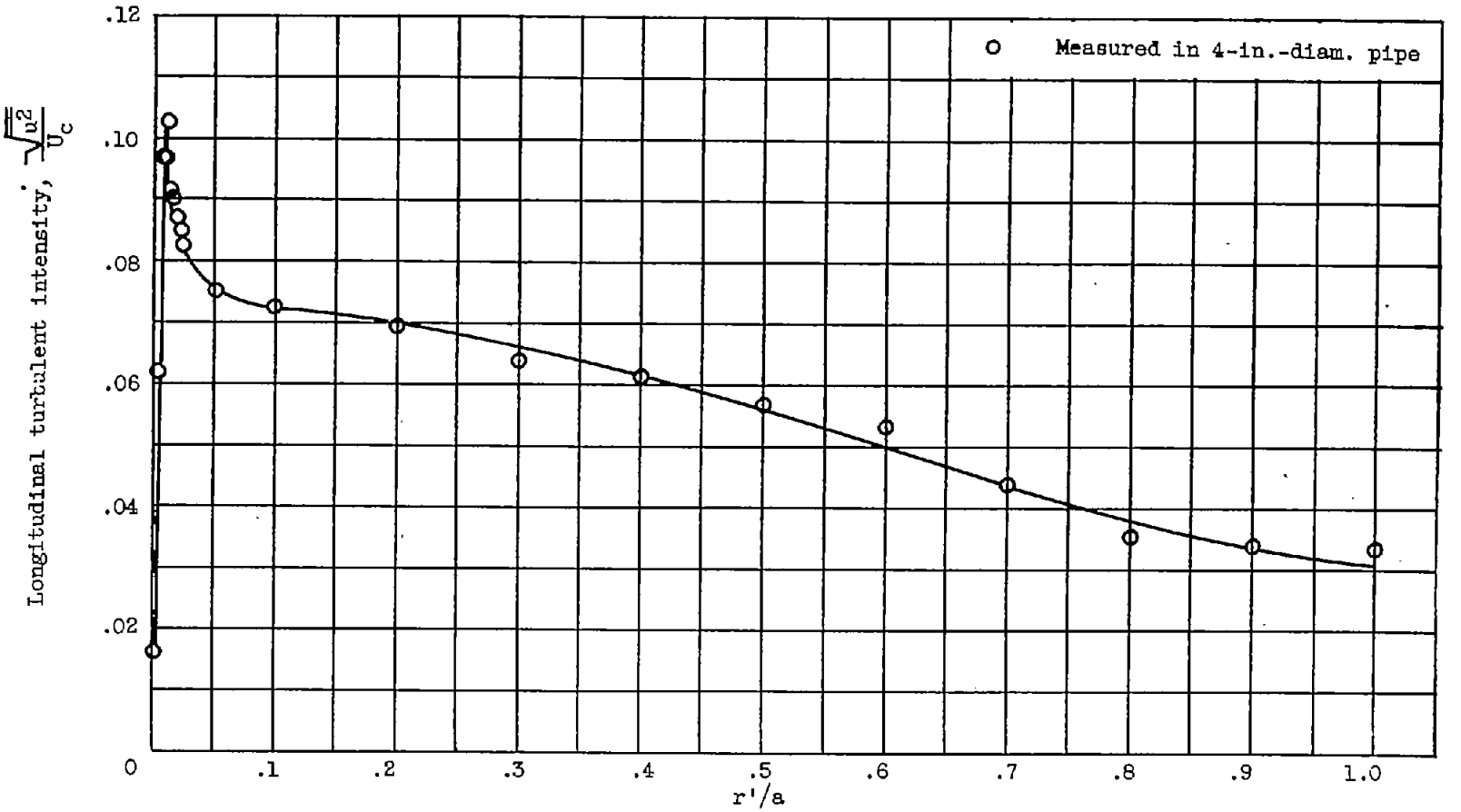

(b) Reynolds number, 50,000.

Figure 13. - Continued. Longitudinal turbulent intensity distribution across pipe.

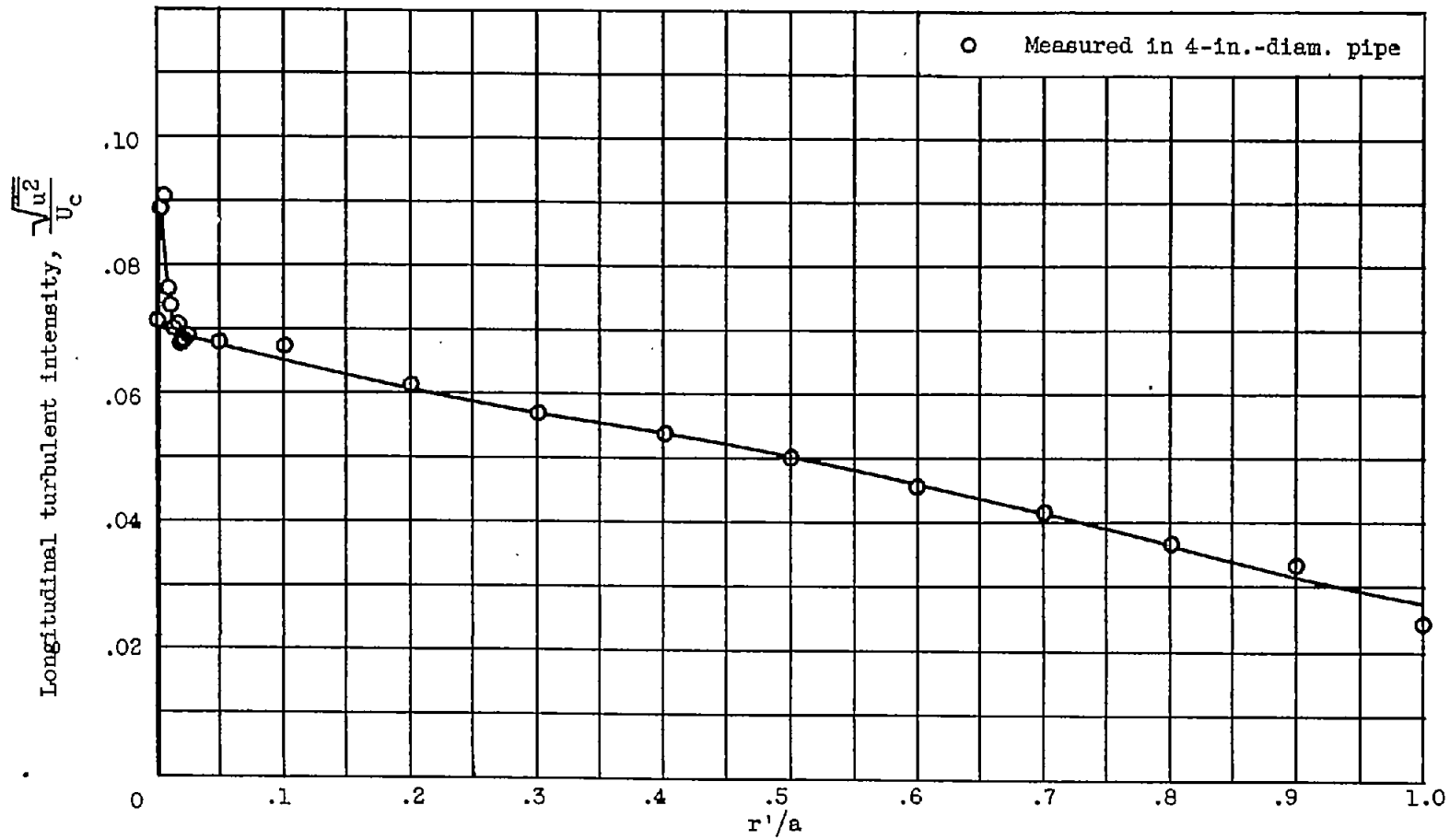

(c) Reynolds number, 100,000

Figure 13. - Continued. Longitudinal turbulent intensity distribution across pipe.

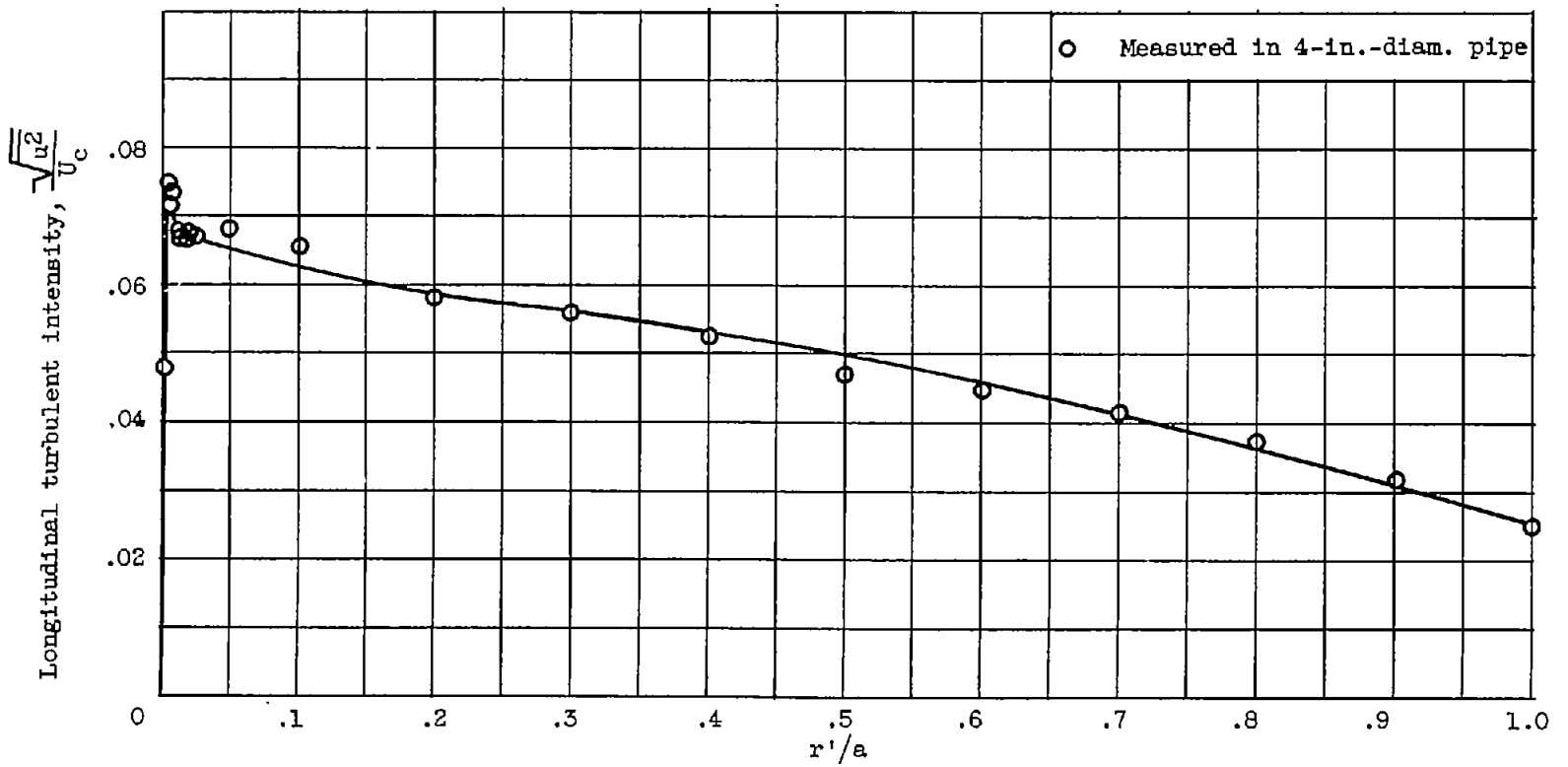

(d) Reynolds number, 150,000.

Figure 13. - Concluded. Longitudinal turbulent intensity distribution across pipe.

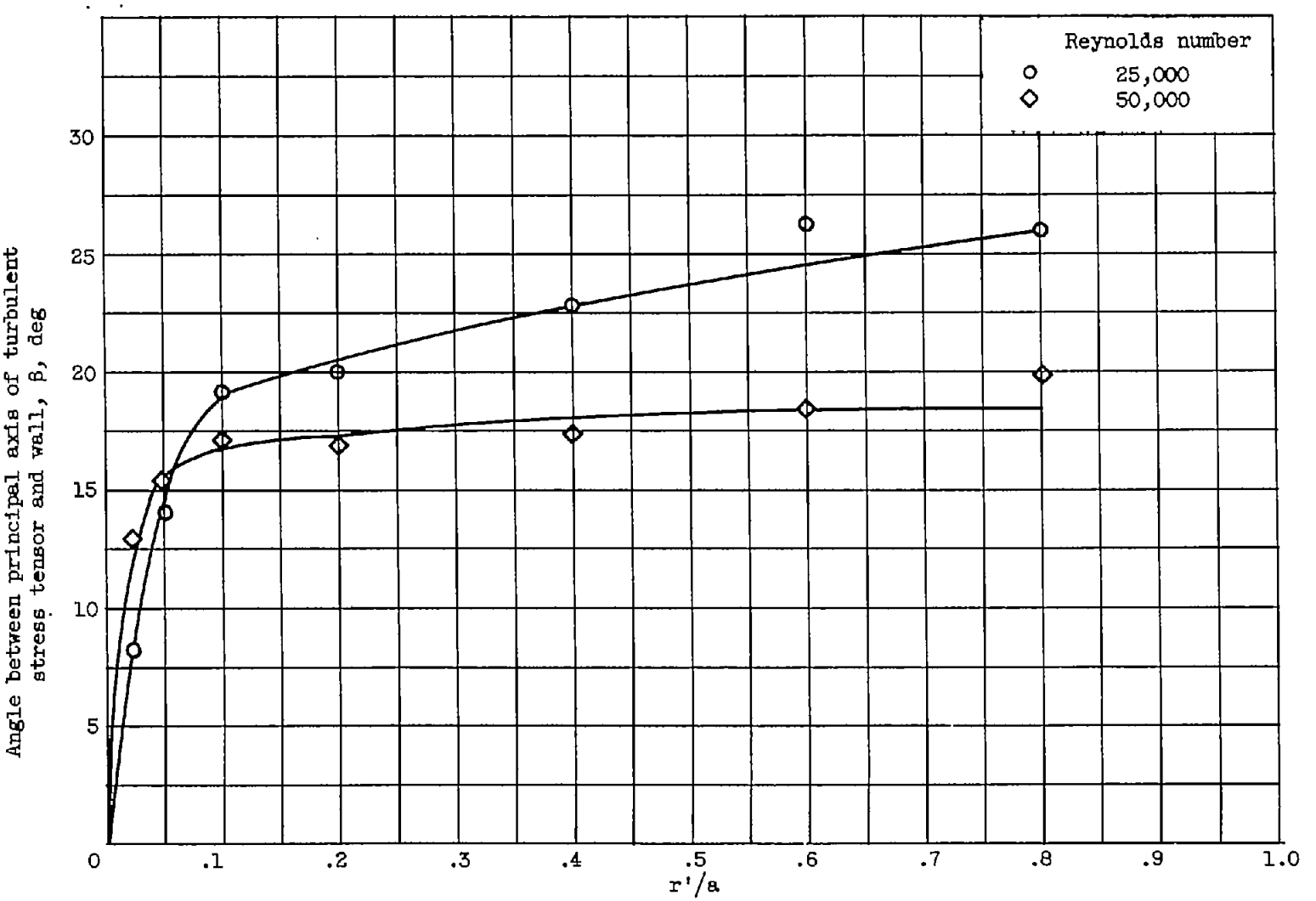

Figure 14. - Variation across pipe of angle between principal axis of turbulent stress tensor and wall.

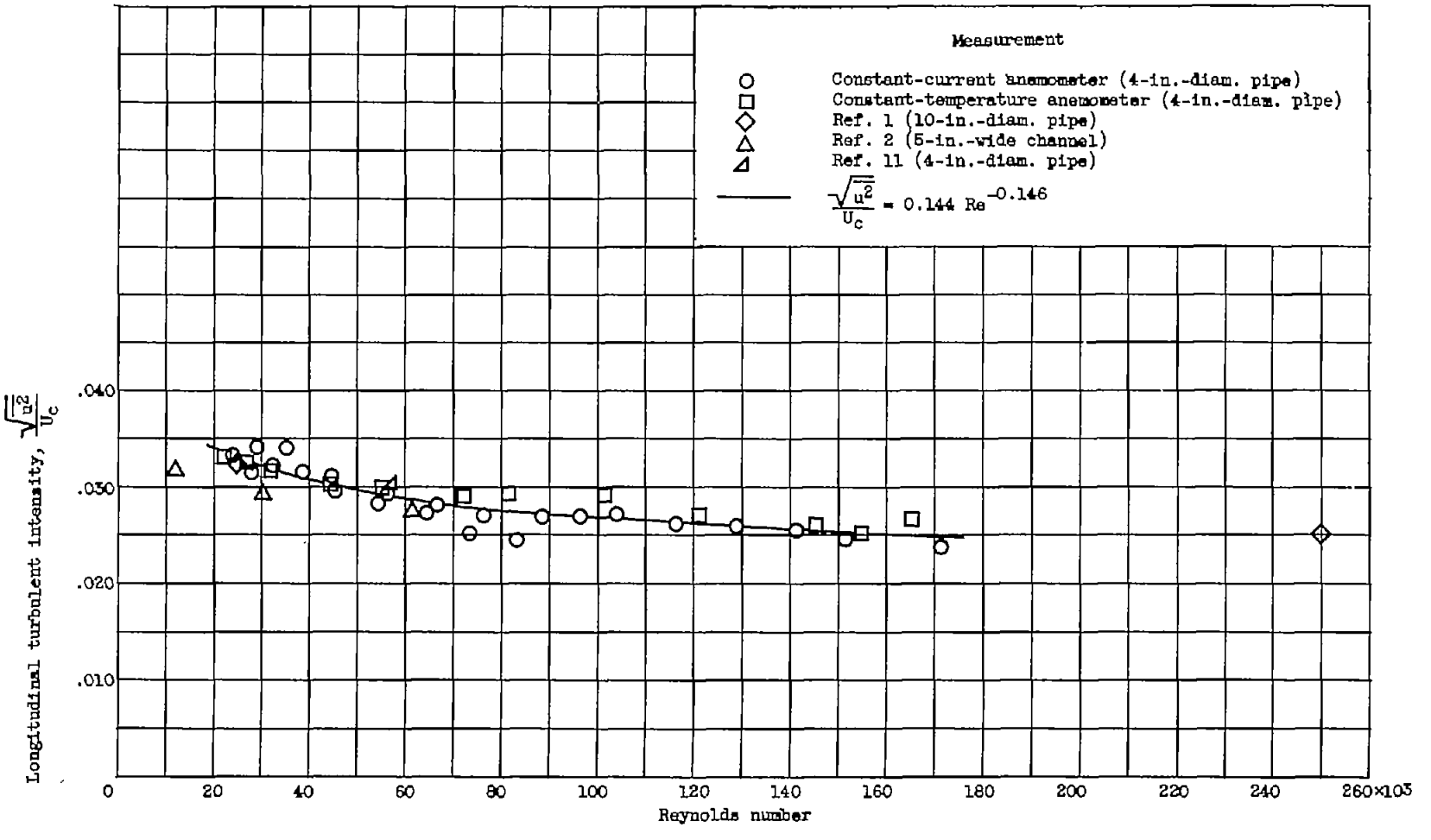

Figure 15. - Longitudinal turbulent intensity at center of pipe.

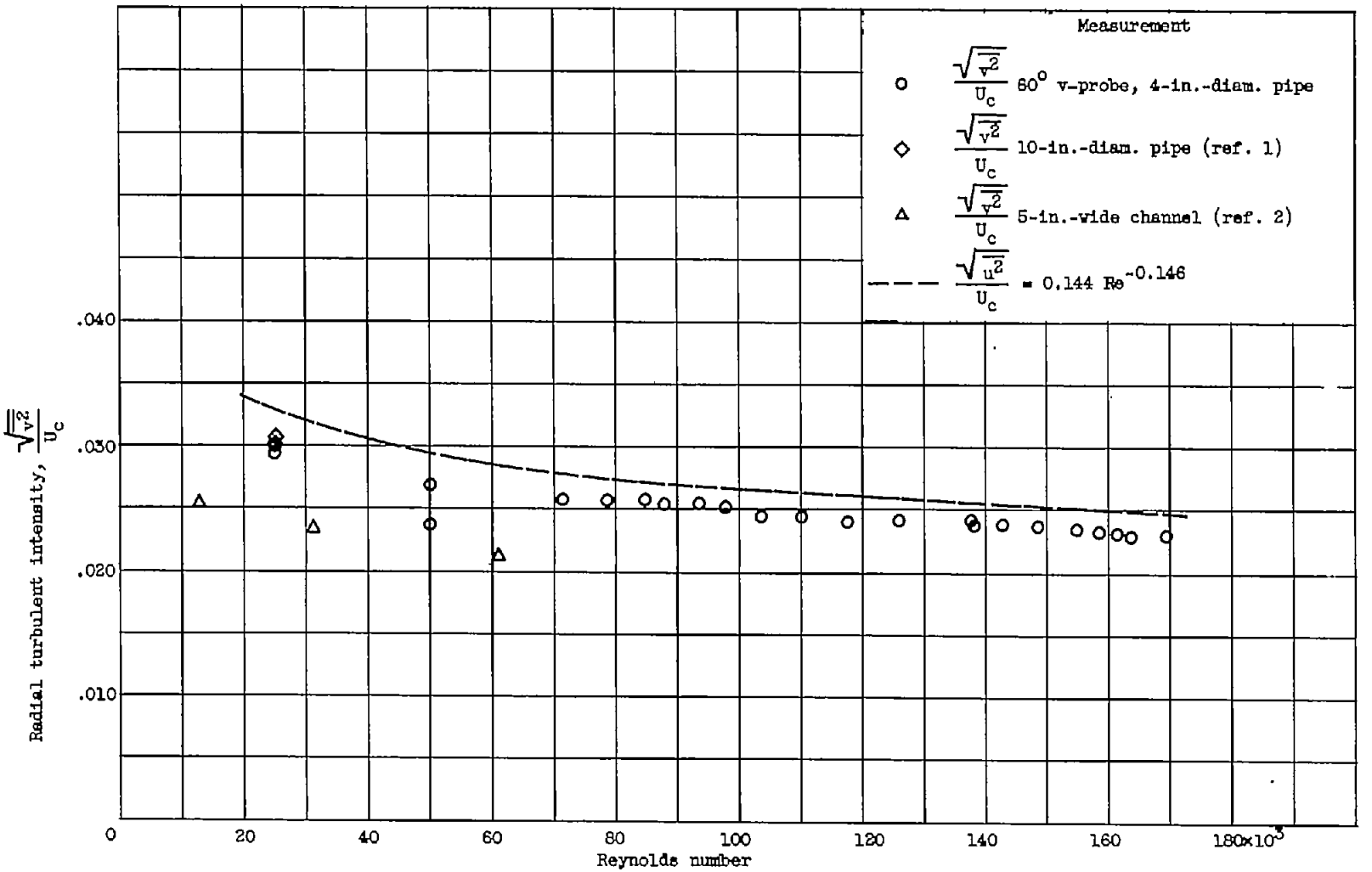

Figure 16. - Radial turbulent intensity at center of pipe.

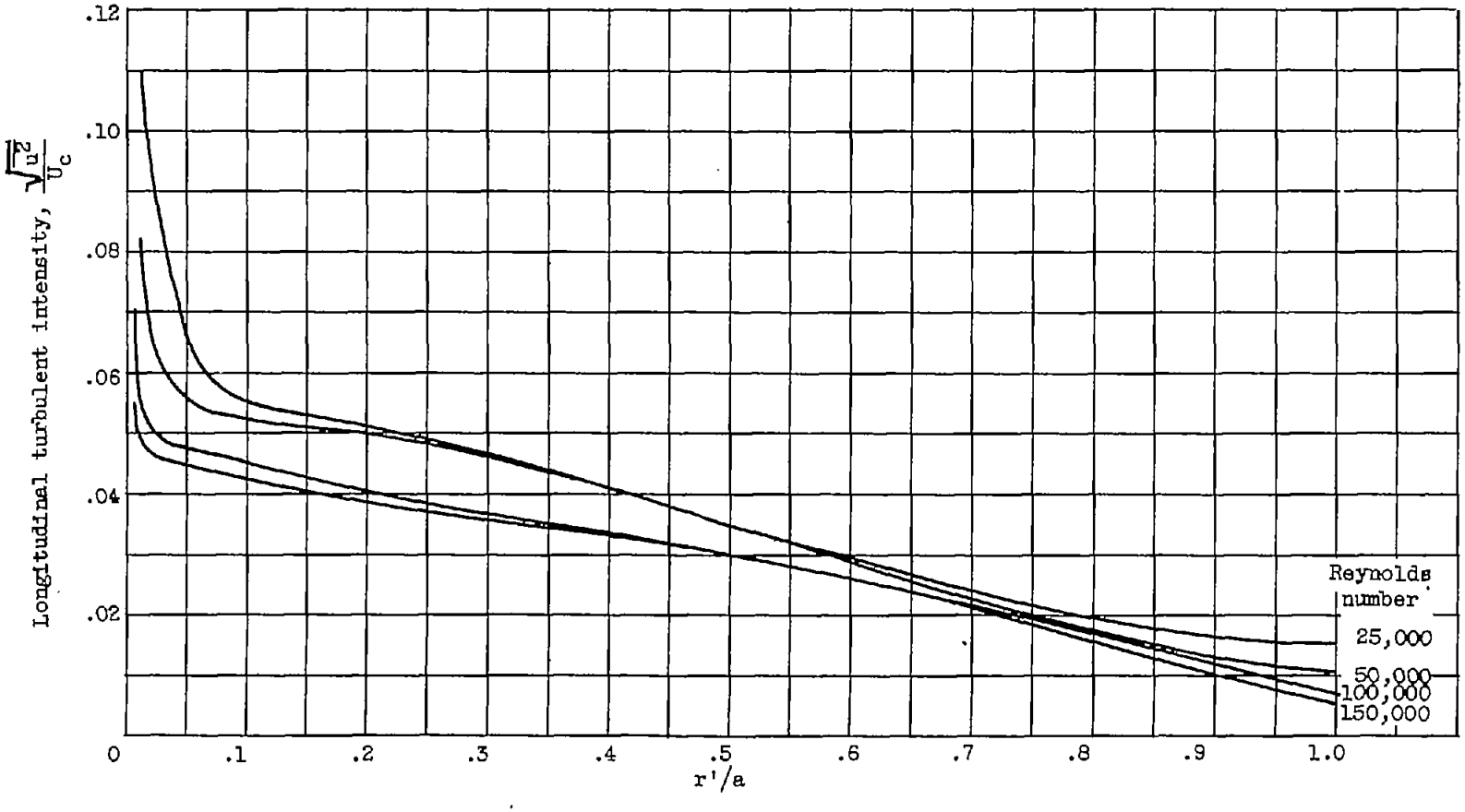

Figure 17. - Longitudinal turbulent intensity distribution across 4-inch pipe with Reynolds number.

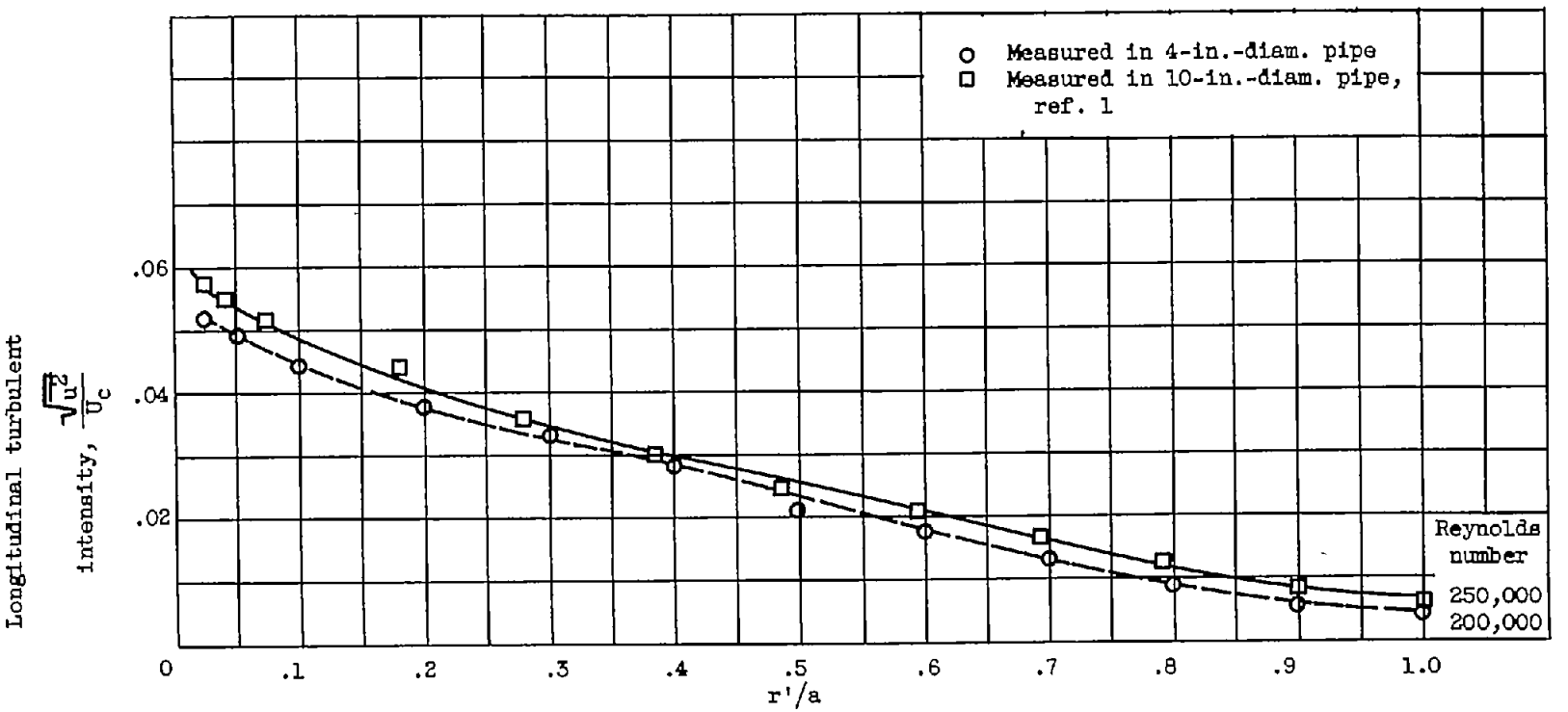

Figure 18. - Longitudinal turbulent intensity distribution across pipe for large Reynolds numbers.

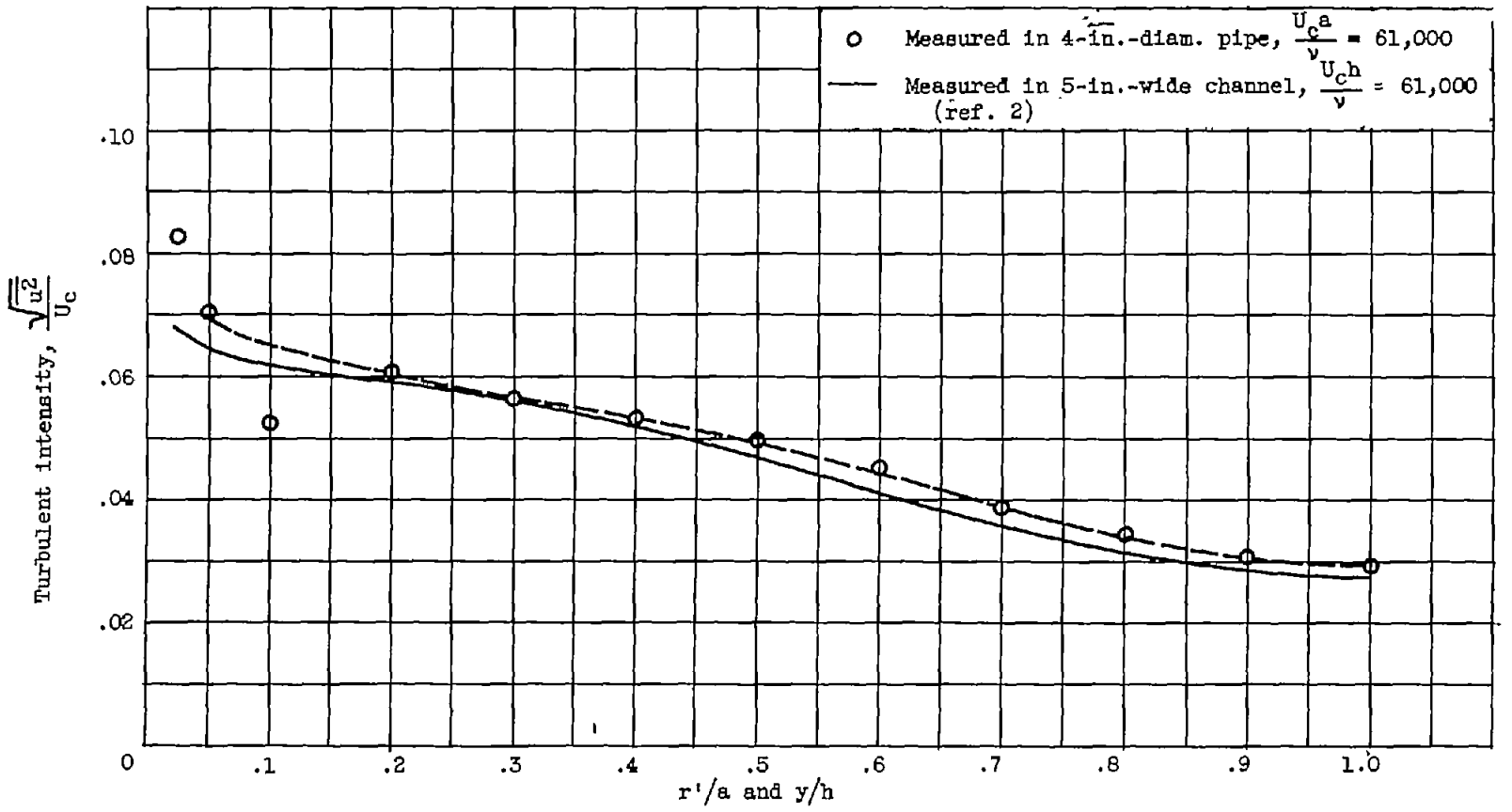

Figure 19. - Comparison of turbulent intensity distributions in pipes and channels.

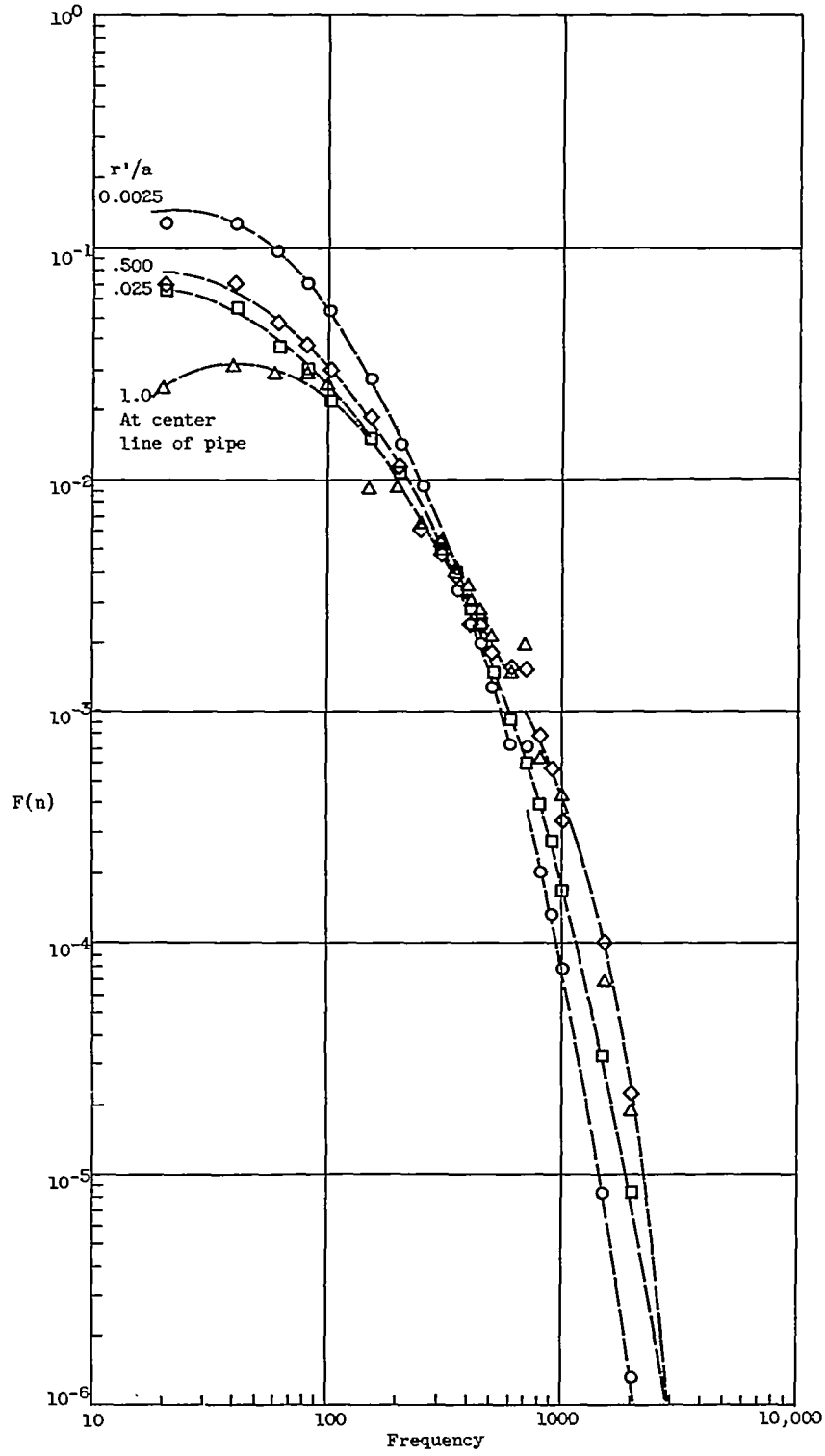

Figure 20. - Spectra of longitudinal turbulent energy. Reynolds number, 25,000.